Source-load Coordinated Optimization Framework for Distributed Energy Systems Using Quasi-potential Game Method

Guofeng Wang, Bei Jiang, Yuchen Liu, Licheng Wang, Youbing Zhang, Jun Yan, and Kai Wang

***Abstract*—Addressing carbon reduction in the energy sector is crucial in the global fight against climate change. In response to this, a source-load coordinated optimization framework is proposed for distributed energy systems (DES). The high carbon-emitting power plants in the source side are transformed into carbon capture power plants to capture CO_2 generated during power generation, thereby improving the power efficiency and decreasing the carbon emissions of the DES. On the load side, the low carbon demand response (LCDR) method is introduced to replace the traditional price-driven demand response. Governed by dynamic carbon emission factors, LCDR aims to facilitate a low carbon shift in end users' energy consumption patterns. An extensive analysis is conducted on the viability of the proposed source-load coordinated framework for low-carbon economic scheduling and an optimal optimization model is formulated by considering the comprehensive cost of the DES. The original problem is then transformed into a hierarchical Stackelberg game model with multi-leaders and multi-followers, which is further solved by an efficient quasi-potential game (QPG) algorithm. The practicality and scalability of the proposed work are validated through simulations conducted on the modified IEEE39-node and IEEE118-node test systems. The findings verify that the proposed framework is highly effective in improving power plant efficiency, optimizing the use of renewable energy, and substantially lowering carbon emissions.**

***Index Terms*—Carbon capture power plant, low-carbon demand response (LCDR), source-load coordinated framework, low-carbon economic scheduling, quasi-potential game (QPG).**

Received: March 20, 2024
Accepted: June 7, 2025
Published Online: September 1, 2025

Guofeng Wang, Bei Jiang, Yuchen Liu, Licheng Wang (corresponding author), and Youbing Zhang are with the College of Information Engineering, Zhejiang University of Technology, Hangzhou 310023, China (e-mail: wgf@zjut.edu.cn; 211123030039@zjut.edu.cn; lyc592575@163.com; wanglicheng@zjut.edu.cn; youbingzhang@zjut.edu.cn).

Jun Yan is with the Security Research Centre, Concordia Institute for Information Systems Engineering, Montreal H3G 2W1, Canada (e-mail: jun.yan@concordia.ca).

Kai Wang (corresponding author) is with the School of Electrical Engineering, Qingdao University, Qingdao 266000, China (e-mail: wkwj888@163.com).

DOI: 10.23919/PCMP.2024.000161

I. Introduction

Global warming, acknowledged by the scientific community as a significant threat to human civilization [1], presents a complex array of environmental, social, and economic challenges. The Paris Agreement sets a target to keep warming between 1.5 ℃ and 2 ℃. However, the global temperature has already risen by about 1.1 ℃ by 2023 [2]. This increase is mainly driven by high CO_2 emissions, highlighting the need for strategies to reduce carbon emissions for a sustainable future. Electricity power sector is a key source of these emissions, responsible for approximately 40% of the global total, more than any other major sources. Thus, reducing carbon emissions in the power sector is crucial for addressing climate change.

Carbon capture and storage (CCS) technology is the core means to reduce emissions with net-zero carbon objectives, and its role is reflected in decarbonizing industries that are difficult to reduce emissions [3], technical support for negative emissions [4] and energy transformation bridge [5]. In the energy sector, the integration of CCS technology in transforming traditional coal-fired power plants into carbon capture power plants (CCPPs) not only markedly reduces carbon emissions but also provides these plants with greater operational flexibility. This improvement substantially enhances the integration of renewable energy sources (RES) [6], while also plays a pivotal role in scenarios where the grid is not required to accommodate surplus RES generation [7] or operates under significant uncertainty [8]. A single CCPP, however, is difficult to achieve the best effect of the system.

Substantial research has been conducted on optimizing the source side of the distributed energy system (DES), aiming to enhance its overall energy efficiency and economic benefits. A carbon cycle system that incorporates power-to-gas (P2G), carbon capture, and supercritical CO_2 processes is developed to increase the energy transformation efficiency of integrated energy systems [9]. Study on two-stage planning models for combined power and gas systems, taking into account uncertainties such as global carbon tax, carbon

prices, and load, demonstrates effectiveness, robustness, and sensitivity [10]. A novel concept called committed carbon emission operation region (CCEOR) of integrated energy systems is proposed, which can characterize the low-carbon feasible space (LCFS) visually [11]. Furthermore, a novel tri-dimensional equilibrium-based stochastic optimal dispatching model is proposed in [12], offering decision-makers effective tools for addressing multi-objective dispatching challenges in DES. The above studies contribute greatly to the low carbon optimization of DES, but they ignore the effect of load side response on the low carbon level.

In the context of rapid advancements in RES and CCS technologies, several governments, notably China [13] and Canada [14], have recently launched "carbon peaking and carbon neutrality" action plans. Experts highlight the vital role of harnessing demand response (DR) potential in the load side, particularly for managing energy consumption [15] and enhancing power system resilience [16]. In [17], an integrated demand response exchange mechanism is proposed, which incorporates seasonal variations and uncertainties. The study demonstrates its effectiveness in emission reduction and emphasizes the economic advantages of an innovative low-carbon dispatching approach. Addressing the prevailing uncertainty in coordinated dispatching of economy and carbon emissions in integrated electricity and heat systems, a multi-objective optimization model is devised that synergizes CCPPs with multi-energy demand response mechanisms [18]. This approach not only fosters RES generation but also significantly contributes to the reduction of CO_2 emissions. At present, research on comprehensive DR and price-based DR is extensive. However, different types of DR often have varying objectives and requirements, and these studies frequently overlook the critical aspect of carbon emissions.

In summary, current research in this area predominantly focuses on one-sided modeling and optimization, targeting either the source or load side to improve the economic efficiency of the DES. However, the inverse relationship between economic dispatch and carbon emission reduction presents a notable challenge in achieving an optimization that balances energy and carbon benefits. These studies frequently fail to comprehensively examine the impact of economic behavior on carbon emissions. Furthermore, the rising penetration of RES, characterized by their inherent variability and uncertainty, exposes the shortcomings of conventional optimization approaches in DES. Reference [19] proposes an accelerated prediction-correction-based alternating direction method of multipliers (PCB-ADMM) algorithm to derive the optimal scheduling strategy of multi-microgrid system (MMGS) in a distributed manner, ensuring the privacy preservation of individual microgrids. However, as an improved algorithm of the traditional ADMM, it is often difficult to verify the existence of the Nash equilibrium point in its game process. This research in [20] adopts the single-leader single-follower Stackelberg game, and proposes a transactive energy management method for a multi-energy microgrid (MEMG) to simultaneously provide optimal energy scheduling and pricing strategies for the MEMG operator.

In response to these challenges, this paper introduces a source-load coordinated optimization framework for low-carbon economic dispatch, integrating a low-carbon demand response (LCDR) and a quasi-potential game (QPG) approach. Different from the multi-agent hierarchical Stackelberg game and QPG, research in [21] adopts an asymmetric Nash bargaining method to ensure the fair allocation of benefits and maintain the willingness of individual MEMGs to participate in cooperation. In [22], bases on Stackelberg-Nash asymmetric bargaining game of genetic algorithm, a multi-operator two-layer optimal scheduling model is established. The key contributions of this research are summarized as follows.

1) Diverging from traditional electricity price-driven mechanisms, the proposed approach is grounded in a carbon-centric perspective, establishing a practical LCDR method that integrates a tiered carbon trading system with comprehensive carbon quotas. This method utilizes a novel full-node carbon potential calculation to determine the dynamic carbon emission factor (DCEF) for the DES. By using DCEF as guiding signals, it aims to direct users towards a low-carbon energy consumption trend, thereby enhancing the load side's low-carbon economic performance.

2) The flexible operation of CCPP on the source side and LCDR on the load side are coordinated within a hierarchical Stackelberg game-based economic optimization framework. The upper layer of this framework operates on a tiered carbon trading model, targeting cost minimization for the source side and optimizing the electricity generation schedules of various power units. The lower layer focuses on maximizing the interests of the load side, adjusting energy consumption plans based on DCEF to fully leverage the low-carbon advantages of both sides.

3) The original optimization problem of hierarchical multi-leader multi-follower Stackelberg game framework is transformed into a QPG model. The existence of the Nash equilibrium of this game model is proved, and the consistency of the Nash equilibrium solution with the optimal solution of the model is demonstrated. Furthermore, by benchmark analysis in typical cases, it concludes that the solution time for algorithms in the DES of different scales shows linear growth, with the time complexity of the algorithms approaching $O(n)$.

The structure of this paper is as follows. Section II explores the low-carbon potential of the source-load coordinated optimization framework by integrating

CCPP and LCDR in the DES scheduling. Section III elaborates on the construction of this framework using a QPG algorithm. Section IV demonstrates the effectiveness and superiority of the proposed framework and algorithm through case studies in typical scenarios, while the scalability in larger node systems is examined. Finally, Section V presents the conclusions.

II. Low-carbon Potential Analysis of the Source-load Coordinated Framework

This paper further extends our previous work [23] to a practical DES with a high penetration of RES, as illustrated in Fig. 1. A source-load coordinated framework is proposed, where the source side is made up of CCPPs, conventional thermal (coal-fired) power plants, wind turbines (WTs), and photovoltaic systems (PVs). In particular, the CCPPs feature solution storage tanks, facilitating peak shaving and valley filling through the temporal shift of energy consumption.

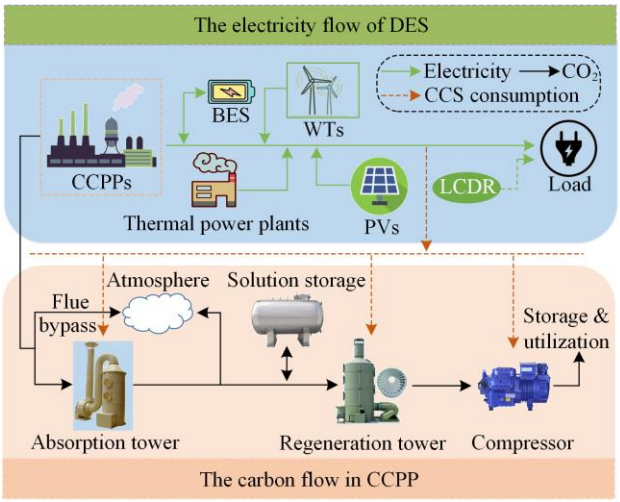

Fig. 1. Diagram of DES framework and energy flows.

A. Flexible Operation Mode of CCPPs

In this study, a flexible operation mode for CCPPs is introduced through the integration of solution storage. This approach allows the monoethanolamine (MEA) solution to absorb CO_2 during peak load periods, with subsequent storage in a dedicated solution tank. In trough periods, the accumulated CO_2 is then transferred to the regeneration tower for extraction and capture [24]. This strategy markedly enhances CO_2 capture efficiency, extends the net output range of CCPPs, and promotes greater utilization of RES [25].

Taking into account the actual power requirements of DES, the energy consumptions in the flexible operation mode of CCPPs are defined as follows:

$$P_{i,t}^{\mathrm{G}} = P_{i,t}^{\mathrm{net}} + P_{i,t}^{\mathrm{ccs}} + P_{i}^{\mathrm{fix}} \tag{1}$$

$$P_{i,t}^{\mathrm{ccs}} = \omega_i \times E_{i,t}^{\mathrm{ccs}} \tag{2}$$

$$E_{i,t}^{\mathrm{ccs}} = \beta_i \times \delta_i \times E_{i,t}^{\mathrm{G}} + E_{i,t}^{\mathrm{S}} \tag{3}$$

$$E_{i,t}^{\mathrm{G}} = e_i \times P_{i,t}^{\mathrm{G}} \tag{4}$$

$$0 \leqslant \delta_i \leqslant 1 \tag{5}$$

where $P_{i,t}^{\mathrm{G}}$ represents the total power consumption of the coal-fired power plant unit i in period t, it is primarily allocated into three categories when unit i is transformed into a CCPP: net output $P_{i,t}^{\mathrm{net}}$, carbon capture energy consumption $P_{i,t}^{\mathrm{ccs}}$, and fixed energy consumption P_{i}^{fix}, and it should be noted that the $P_{i,t}^{\mathrm{ccs}}$ and P_{i}^{fix} will be 0 when unit i represents a conventional coal-fired power plant; $P_{i,t}^{\mathrm{ccs}}$ is directly correlated with the total mass of CO_2 captured, $E_{i,t}^{\mathrm{ccs}}$, at time t, with ω_i representing the coefficient for carbon capture energy consumption; $E_{i,t}^{\mathrm{ccs}}$ includes both the CO_2 from power generation, $E_{i,t}^{\mathrm{G}}$, and the CO_2 from solution storage tank, $E_{i,t}^{\mathrm{S}}$; β_i represents the capture coefficient of CO_2; δ_i denotes the split ratio of flue/gas and δ_i for CCPPs should be maintained within a range of 0 to 1; and $E_{i,t}^{\mathrm{G}}$ is proportional to $P_{i,t}^{\mathrm{G}}$ with the carbon emission intensity e_i.

To realize the flexible operation mode for the CCPPs, the solution storage tank is introduced in this work, where CO_2 dissolves in MEA and becomes a liquid compound. The mass of CO_2 extracted from the solution storage tank is calculated based on the volume of the solution [26]. The modeling of this essential component is elaborated in the followings [27]:

$$V_{i,t}^{\mathrm{S}} = \frac{E_{i,t}^{\mathrm{S}} \times M_{\mathrm{mea}}}{M_{\mathrm{co_2}} \times \eta_i \times N_{\mathrm{mea}} D_{\mathrm{mea}}} \tag{6}$$

where $V_{i,t}^{\mathrm{S}}$ denotes the volume of solution required for CO_2 extraction at time t in CCPPi; the molar masses of MEA (M_{mea}) and CO_2 ($M_{\mathrm{co_2}}$) are the key to understanding their interactions; the CO_2 extraction efficiency of the tower is represented by η_i; furthermore, the concentrated volume of MEA is indicated as N_{mea} and its density is indicated by D_{mea}. Equation (6) represents the relationship between CO_2 mass and MEA solution volume. The corresponding constraints are as follows:

$$\begin{cases} V_{i,t}^{+} = V_{i,t-1}^{+} - V_{i,t}^{\mathrm{S}} \\ V_{i,t}^{-} = V_{i,t-1}^{-} + V_{i,t}^{\mathrm{S}} \end{cases} \tag{7}$$

$$\begin{cases} 0 \leqslant V_{i,t}^{+} \leqslant V_i \\ 0 \leqslant V_{i,t}^{-} \leqslant V_i \end{cases} \tag{8}$$

$$\begin{cases} V_{i,0}^{+} = V_{i,24}^{+} \\ V_{i,0}^{-} = V_{i,24}^{-} \end{cases} \tag{9}$$

where $V_{i,t}^{+}$ and $V_{i,t}^{-}$ represent the volumes of these solutions, respectively; the capacity of the solution storage tank in each unit is denoted as V_i. Equation (7) describes the dynamic volumes of the rich and lean MEA solutions in the storage tank at any given time t. Equation (8) establishes the operational volume limits for both rich and lean solutions. Finally, Equation (9) dictates that the solution volumes should remain constant after a 24-hour period.

B. Low-carbon Mechanism Based on LCDR

Price-based demand response (PDR) [28] and incentive-based demand response (IDR) [29] are strategies that are widely utilized by researchers to enhance demand-side scheduling. Both approaches contribute significantly to lowering system CO_2 emissions by encouraging users to adjust their behaviors of electricity consumption in response to price signals. Despite these benefits, there is an inherent tension between achieving economic efficiency and reducing carbon emissions within the power system and the broader energy sector.

To address this, the LCDR method is introduced that leverages the DCEF to make changes in electricity consumption behaviors [30]. By guiding users to adjust their power use, LCDR directly influences the carbon emissions footprint of the DES. Users utilize the DCEF to understand the indirect carbon emissions associated with their electricity usage [31]. The definition of LCDR method is detailed below, focusing on its application within the DES. At its core, the source side of the DES delivers electrical energy to meet end-user's demand. Simultaneously, it transfers carbon emission responsibility to end-users through carbon flow mechanisms, thereby fostering a sense of shared accountability for emissions generated during energy production. This method is grounded in the theory of carbon emission flow analysis, which adeptly maps the link between carbon emissions on the source side and electricity usage on the load side [32]. A schematic illustrating the low-carbon operation mechanism of the LCDR, including carbon emission flows within the power system, is shown in Fig. 2.

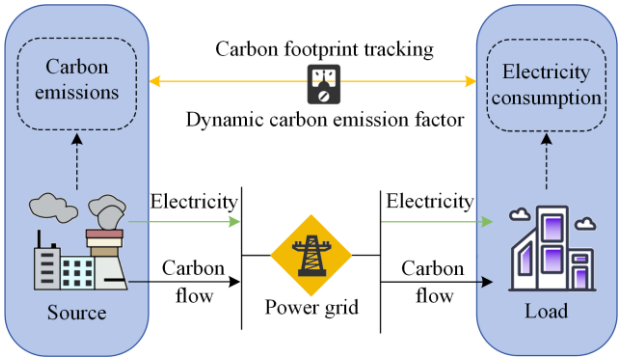

Fig. 2. The low-carbon mechanism of LCDR.

As can be seen, the DCEF is instrumental in the LCDR method, serving as a critical component. Specifically, the DCEF within LCDR is derived by averaging the spatial load in accordance with the carbon potential of each node, as delineated as:

$$\mathcal{F}_t = \sum_{j \in Z} (P_{j,t}^{\text{load}} \times \mathcal{E}_{j,t}) \Big/ \sum_{j \in Z} P_{j,t}^{\text{load}} \tag{10}$$

where $\mathcal{F}_t$ represents the DCEF of the DES at time t; Z is the set of all nodes in the DES; $P_{j,t}^{\text{load}}$ is the load of node j at time t; and $\mathcal{E}_{j,t}$ represents the carbon potential of the j node at time t.

To specify the computation of $\mathcal{E}_{j,t}$, the methodology for calculating the carbon potential is explored. Typically, this calculation is a straightforward multiplication of the power output from power plants by their respective carbon emission intensities. However, this approach is refined with the incorporation of CCPPs to capture CO_2. When CO_2 is captured by CCPPs at time t, the carbon potential associated with the nodes linked to these plants will decrease. Assuming that coal-fired power plants i and RES i are interconnected with node j, the improved carbon potential for this node at time t is articulated as:

$$\mathcal{E}_{j,t} = \frac{\sum_{s \in J^{+}} P_{sj,t}^{\text{flow}} \times \mathcal{E}_{s,t} + (1 - \beta_j \delta_j) \times P_{j,t}^{\text{G}} e_j^{\text{G}}}{\sum_{s \in J^{+}} P_{sj,t}^{\text{flow}} + P_{j,t}^{\text{G}} + P_{j,t}^{\text{res}}} \tag{11}$$

where J^{+} represents the set of all nodes connected to node j; $P_{sj,t}^{\text{flow}}$ represents the power flow from node s to node j at time t; $P_{j,t}^{\text{G}}$ and $P_{j,t}^{\text{res}}$ are the power generated by unit i and RES power input to j at the time t, respectively; and e_j^{G} is the carbon emission factor of coal-fired units at node j.

C. Analysis of Source-load Coordinated Low-carbon Mechanism

It is evident that the CCPPs with a comprehensive flexible operation mode on the source side, along with the LCDR method on the load side, independently contribute to the low-carbon operation of the DES. However, these approaches exhibit specific limitations.

CCPPs serve as the primary low-emission power generation units that address peak load demands. Given their operational characteristics, these units frequently operate at or near their maximum capacity, resulting in insufficient capacity to meet additional or sudden backup power requirements. This limitation requires the activation of additional units of high-carbon emission to fulfill reserve requirements, thereby increasing the overall carbon emissions of the DES [33]. In this case, the strategic incorporation of LCDR method on the load

side presents a promising solution to this challenge. By effectively reducing peak demand, LCDR can avoid the extra support of the high-emission backup units. Thus, the collaborative integration of LCDR with the flexible operational capabilities of CCPPs significantly amplifies the low-carbon advantages of the system. This strategic combination marks a pivotal advancement in enhancing the environmental sustainability of the DES.

Configuring the system with LCDR alone enables a strategic redirection of peak loads to off-peak times, fulfilled by RES with net-zero carbon emission, thus lowering the DES's carbon footprint [34]. However, in scenarios where RES output is insufficient, the shifted demand often falls back on higher-emission generators, undermining the DES's low-carbon advantage. The deployment of CCPPs in this circumstance offers a solution by catering to the redistributed demand with their inherently low emissions. This adaptation ensures a sustained reduction in carbon emissions, especially during times when RES cannot meet the load requirements in the DES, thereby securing the system's low-carbon purpose.

This study contributes to low-carbon scheduling in DES by introducing a coordinated framework that leverages the strengths of CCPPs on the supply side and the LCDR approach on the demand side. Building on our previous research [23], real-world data are utilized to construct and present a schematic diagram, as demonstrated in Fig. 3. This diagram serves as preliminary evidence that integrating LCDR methods with CCPPs can significantly enhance net power output, addressing the carbon reduction limitations of each approach when considered in isolation.

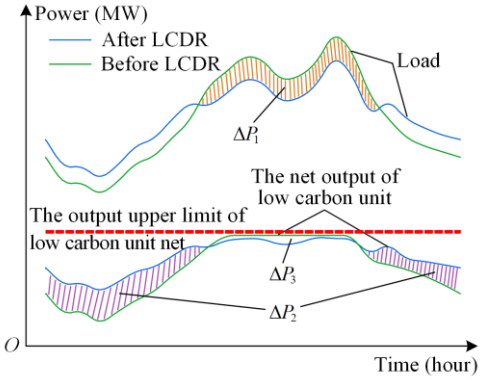

Fig. 3. Schematic diagram of the mechanism of LCDR.

In summary, the framework aims to maximize the collective carbon mitigation capabilities of these methods, thereby promoting an economically promising and environmentally sustainable operation of DES.

III. Low-carbon Source-load Coordinated Framework

In Section II, the source-load coordinated mechanism has been analyzed and the low carbon scheduling potential of the proposed framework has been explored. In this section, the detailed formulations of this framework and the algorithm for solving the problem are described. The specific framework of the LCDR-based source-load coordinated scheduling is shown in Fig. 4.

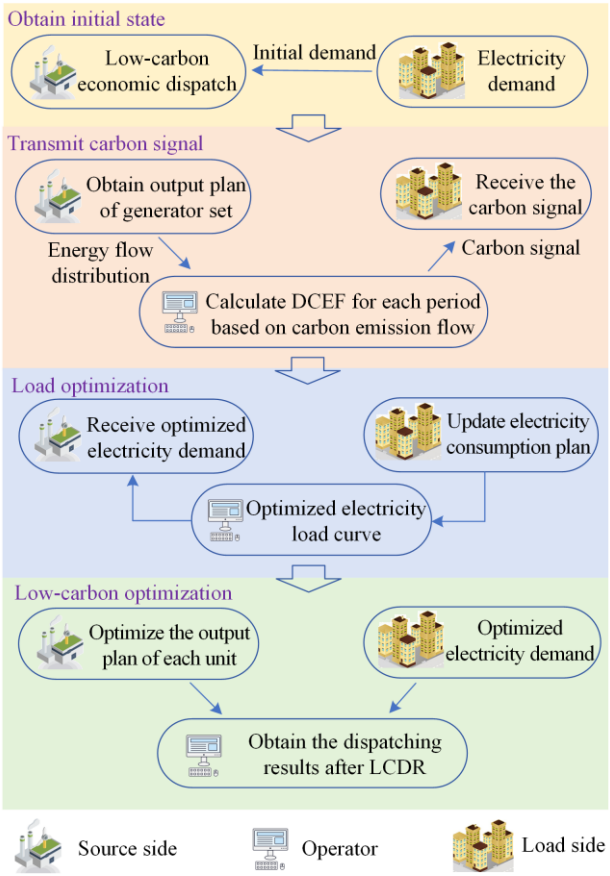

Fig. 4. Framework of the source-load coordinated dispatching.

The interaction indicates a game-theoretic relationship between source and load decisions. Considering this complex interplay, a hierarchical decision-making model is developed based on the Stackelberg game, incorporating a quasi-potential function-based method. This model aims at coordinated optimization in power generation and load scheduling, a concept to be elaborated in the following Section III.C. Initially, on the source side, the specific problem is formulated as an optimal scheduling model, as follows.

A. Optimal Scheduling Model on the Source Side

1) Objective Function on the Source Side

The source side comprises the output of traditional coal-fired power plants, CCPPs and RES, to meet the total load demand. An optimization scheduling model is established with the primary objective of minimizing the overall operational costs for the source side in the DES, denoted as φ_i^1, of which the payoff function is given by:

$$\varphi_i^1 = C_1 + C_2 + C_3 + C_4 + C_5 + C_6 + C_7 \tag{12}$$

where C_1 and C_2 represent the generation and start-stop costs of coal-fired power plants, respectively; C_3 denotes the penalty cost associated with reductions in RES power, accounting for the stochastic nature of RES power output; C_4 corresponds to the loss cost incurred during CCS; and C_5 is identified as the daily depreciation cost of CCPPs. The detailed formulations of each cost component are presented as:

$$C_1 = \sum_{i=1}^{N_g}\sum_{t=1}^{24} X_{i,t} \times \left[a_i (P_{i,t}^{G})^2 + b_i P_{i,t}^{G} + c_i \right] \tag{13}$$

$$C_2 = \sum_{i=1}^{N_g}\sum_{t=1}^{24} \tau \times \left[X_{i,t}(1 - X_{i,t-1}) + X_{i,t-1}(1 - X_{i,t}) \right] \tag{14}$$

$$C_3 = \sum_{t=1}^{24}\sum_{i=1}^{N_{res}} \tau_{re} \times (\hat{P}_{i,t} - P_{i,t}^{res}) \tag{15}$$

$$C_4 = \sum_{i=1}^{N_g}\sum_{t=1}^{24} \tau_{co_2} \times \varphi E_{i,t}^{ccs} \tag{16}$$

$$C_5 = \tau_{ccs} \frac{(1+r)^{Y_1} + r}{365\left[(1+r)^{Y_1} - 1\right]} + \tau_{so} \times V \frac{(1+r)^{Y_2} + r}{365\left[(1+r)^{Y_2} - 1\right]} \tag{17}$$

where N_g denotes the number of coal-fired units; the variable $X_{i,t}$ represents the operating state of unit i at time t, taking Boolean values of 0 or 1; the coefficients a_i, b_i, and c_i are associated with the coal cost factors for unit i; τ signifies the cost coefficient for starting/stopping operations; N_{res} indicates the number of RES units, i.e., PVs and WTs; the penalty cost coefficients for RES are given by τ_{re}; $\hat{P}_{i,t}$ and $P_{i,t}^{res}$ represent the forecasted and actual power output of RES units, respectively; the coefficient τ_{co_2} corresponds to the cost of the solvent in CCS processes; φ denotes the loss during solvent operations; the depreciation rate for CCPP equipment is expressed by r; the cost coefficient of CCS equipment (without solution storage) and the solution storage are indicated by τ_{ccs} and τ_{so}, respectively; Y_1 and Y_2 refer to the lifespan for depreciation of CCS equipment and solution storage, respectively; and V means the volume of solution storage.

In line with the global transition toward incorporating market mechanisms into power system reforms to balance low-carbon goals with economic development, this study introduces a practical carbon trading mechanism on the supply side. This approach is characterized by models of tiered carbon pricing, detailed in (18), and a carbon trading quota system, as outlined in (19). These models collectively aim to enhance energy efficiency and reduce emissions in power generating units, contributing to the broader global trend [35]:

$$C_6 = \begin{cases} \lambda \times q, & q < l \\ \lambda \times \left[q + \alpha(q - l) \right], & l < q \leqslant 2l \\ \lambda \times \left[q + \alpha(2q - 3l) \right], & 2l < q \leqslant 3l \\ \cdots \end{cases} \tag{18}$$

$$q = E^{total} - \sum_{i=1}^{N_g}\sum_{t=1}^{24} \xi \times P_{i,t}^{G} \tag{19}$$

$$C_7 = \sum_{t=1}^{24} \lambda \times \Delta E_t^{lcdr} \tag{20}$$

where λ denotes the basic price of carbon trading; q defines the carbon emissions exceeding the system's allocated quota; l represents the carbon emission interval; α is the rate at which the carbon trading price increases; E^{total} represents the total CO_2 emissions of the DES; and ξ denotes the carbon quota coefficient; meanwhile, ΔE_t^{lcdr} is the reduced carbon emissions; and C_7 describes the incentive cost for carbon reduction after the LCDR method, as provided by the source side. On the source side, rewards for carbon emission reduction are paid to end-users on the load side, based on the carbon emission reduction incentive price λ and the reduced carbon emissions ΔE_t^{lcdr} achieved through LCDR method.

2) Constraints on the Source Side

After LCDR, the output of each generating unit on the source side is adjusted to meet the real-time demand of the load side. Consequently, the power balance constraint for the DES is denoted as follows:

$$\sum_{i=1}^{N_g} P_{i,t}^{net} + \sum_{i=1}^{N_{res}} P_{i,t}^{res} + \sum_{i=1}^{N_b} P_{i,t}^{dch} = P_t^{lcdr} + \sum_{i=1}^{N_b} P_{i,t}^{ch} \tag{21}$$

where N_b denotes the number of battery energy storage (BES) units; $P_{i,t}^{ch}$ and $P_{i,t}^{dch}$ represent the charging and discharging power of the ith BES unit at time t, respectively; meanwhile, P_t^{lcdr} indicates the total load after LCDR at time t.

The corresponding power generation constraints for the coal-fired units are outlined as follows:

$$X_{i,t} \times P_{i,\min}^{G} \leqslant P_{i,t}^{G} \leqslant X_{i,t} \times P_{i,\max}^{G}, \quad i \in N_g \tag{22}$$

$$-R_{i,\max}^{G} \leqslant P_{i,t}^{G} - P_{i,t-1}^{G} \leqslant R_{i,\max}^{G}, \quad i \in N_g \tag{23}$$

$$\begin{cases} \sum_{k=t}^{t+T_i^{off}-1} (1 - X_{i,k}) \geqslant T_i^{off}(X_{i,t-1} - X_{i,t}) \\ \sum_{k=t}^{t+T_i^{on}-1} X_{i,k} \geqslant T_i^{on}(X_{i,t} - X_{i,t-1}), \quad i \in N_g \end{cases} \tag{24}$$

$$0 \leqslant P_{i,t}^{\mathrm{res}} \leqslant \hat{P}_{i,t}, \quad i \in N_{\mathrm{res}} \tag{25}$$

$$-R_{i,\max}^{\mathrm{res}} \leqslant P_{i,t}^{\mathrm{res}} - P_{i,t-1}^{\mathrm{res}} \leqslant R_{i,\max}^{\mathrm{res}}, \quad i \in N_{\mathrm{res}} \tag{26}$$

$$P_{sj,t}^{\mathrm{flow}} = \frac{\theta_{s,t} - \theta_{j,t}}{z_{sj}} \tag{27}$$

$$-P_{sj,\max}^{\mathrm{flow}} \leqslant P_{sj,t}^{\mathrm{flow}} \leqslant P_{sj,\max}^{\mathrm{flow}} \tag{28}$$

$$-\theta_s^{\max} \leqslant \theta_{s,t} \leqslant \theta_s^{\max} \tag{29}$$

$$\theta_{\mathrm{ref}} = 0 \tag{30}$$

where $P_{i,\max}^{\mathrm{G}}$ and $P_{i,\min}^{\mathrm{G}}$ are the upper and lower output limits of the ith coal-fired unit, respectively; $R_{i,\max}^{\mathrm{G}}$ is the upper limits of the climbing speed; T_i^{on} and T_i^{off} are respectively the minimum start-up and shutdown time; $R_{i,\max}^{\mathrm{res}}$ is the upper climbing speed limits of RES i; $\theta_{s,t}$ and $\theta_{j,t}$ are the voltage phase angle of nodes s and j at time t, respectively; z_{sj} is the reactance of the line between node s and node j; $P_{sj,\max}^{\mathrm{flow}}$ is the maximum transmission power of node s to node j; $\theta_s^{\max}$ represents the maximum voltage phase angle limit of node s; and θ_{ref} is the phase angle of the balanced node voltage, which is set to 0.

Constraints (22)–(24) regulate the output and operational cycling of coal-fired units. Constraints (25)–(26) define the output power limitations for RES generation. Lastly, constraints (27)–(30) determine the power flow parameters of the DES.

It is important to note that CCPPs are essentially modifications of traditional coal-fired power plants. Consequently, in addition to meeting the constraints previously specified for coal-fired units, it is crucial to take into account the unique energy consumption models and the constraints related to solution storage for CCPPs. The specific models governing the flexible operation of CCPPs, as introduced in Section II.A, are detailed in (1)–(9).

The operational constraints of the BES [36] are specified as:

$$S_{i,t} = S_{i,t-1} + \kappa_i^{\mathrm{ch}} P_{i,t}^{\mathrm{ch}} - (1/\kappa_i^{\mathrm{dch}}) P_{i,t}^{\mathrm{dch}}, \quad i \in N_{\mathrm{b}} \tag{31}$$

$$0 \leqslant P_{i,t}^{\mathrm{ch}} \leqslant X_{i,t}^{\mathrm{ch}} \times P_{i,\max}^{\mathrm{ch}}, \quad i \in N_{\mathrm{b}} \tag{32}$$

$$0 \leqslant P_{i,t}^{\mathrm{dch}} \leqslant X_{i,t}^{\mathrm{dch}} \times P_{i,\max}^{\mathrm{dch}}, \quad i \in N_{\mathrm{b}} \tag{33}$$

$$0 \leqslant X_{i,t}^{\mathrm{ch}} + X_{i,t}^{\mathrm{dch}} \leqslant 1, \quad i \in N_{\mathrm{b}} \tag{34}$$

$$S_i^{\min} \leqslant S_{i,t} \leqslant S_i^{\max}, \quad i \in N_{\mathrm{b}} \tag{35}$$

$$S_{i,0} = S_{i,24}, \quad i \in N_{\mathrm{b}} \tag{36}$$

where $S_{i,t}$ is the SOC of the BES i at time t; κ_i^{ch} and κ_i^{dch} denote the coefficients for charging and discharging efficiency [37]; $P_{i,t}^{\mathrm{ch}}$ and $P_{i,t}^{\mathrm{dch}}$ represent the charging and discharging power of the BES i at time t; the variables $X_{i,t}^{\mathrm{ch}}$ and $X_{i,t}^{\mathrm{dch}}$ indicate the charging and discharging states of BES i at time t, taking values of 0 or 1; $P_{i,\max}^{\mathrm{ch}}$ and $P_{i,\max}^{\mathrm{dch}}$ are the maximum charging and discharging power, respectively; $S_i^{\min}$ and $S_i^{\max}$ represent the minimum and maximum SOC, respectively.

Equation (31) defines the calculation for the state of charge (SOC) [38] of the BES. Equations (32)–(33) set the charging and discharging power limits. Equation (34) prohibits the BES from charging and discharging simultaneously. The SOC limits are prescribed by (35), and finally, equation (36) ensures that the SOC capacity remains constant after the end of the initial state calibration [39], dynamic charge and discharge scheduling [40], and SOC equalization control [41].

B. LCDR Method on Load Side

1) Objective Function on Load Side

The load side aims to maximize incentive costs after implementing LCDR, as defined by the payoff φ_i^2:

$$\varphi_i^2 = C_7 \tag{37}$$

$$\Delta E_t^{\mathrm{lcdr}} = (\Delta P_{\mathrm{dr},t}^{-} - \Delta P_{\mathrm{dr},t}^{+}) \times \mathcal{F}_t \tag{38}$$

where $\Delta P_{\mathrm{dr},t}^{-}$ represents the decrease; and $\Delta P_{\mathrm{dr},t}^{+}$ represents the increase of load demand due to LCDR during period t. Equation (38) demonstrates how the system's carbon emissions are reduced. This underscores the pivotal role of electricity load demand management in reducing carbon emissions.

2) Constraints on Load Side

The load variation constraints after the implementation of LCDR method are presented as follows:

$$\begin{cases} 0 \leqslant \Delta P_{\mathrm{dr},t}^{-} \leqslant x_t^{-} \times \Delta P_{\mathrm{dr}}^{\max} \\ 0 \leqslant \Delta P_{\mathrm{dr},t}^{+} \leqslant x_t^{+} \times \Delta P_{\mathrm{dr}}^{\max} \end{cases} \tag{39}$$

$$\begin{cases} P_t^{\mathrm{load}} + \Delta P_{\mathrm{dr},t}^{+} \leqslant P_{\max,t}^{\mathrm{load}} \\ \Delta P_{\mathrm{dr},t}^{-} \leqslant P_t^{\mathrm{load}} \end{cases} \tag{40}$$

$$\left| \sum_{t=1}^{24} (\Delta P_{\mathrm{dr},t}^{+} - \Delta P_{\mathrm{dr},t}^{-}) \right| \leqslant \zeta \tag{41}$$

$$x_t^{+} + x_t^{-} \leqslant 1 \tag{42}$$

where x_t^{-} and x_t^{+} represent the state of load decrease and increase at time t, taking Boolean values of 0 or 1; $\Delta P_{\mathrm{dr}}^{\max}$ is the upper limit of load change; $P_{\max,t}^{\mathrm{load}}$ is the maximum allowable load; and P_t^{load} is the initial load before LCDR. Equation (41) represents that the total load change in a single day should be kept within a limit of ζ. Equation (42) describes that load increase and

reduction cannot occur simultaneously.

C. Hierarchical Stackelberg Game Algorithm

As emphasized at the beginning of Section III, the precise modeling of the dynamic and strategic interplay between the supply and load sides within the DES is crucial [42]. The original optimization problem is formulated into a mixed integer nonlinear programming (MINLP) in (12), which is typically nondeterministic polynomial-time (NP)-hard [43] that is difficult to solve. To address this complexity, we employ a hierarchical Stackelberg game model framework with multi-leaders and multi-followers that accounts for the intricate interactions between the source and load sides. Moreover, we prove that the hierarchical Stackelberg game model formulated in this section can be resolved using an efficient QPG approach [44].

1) Hierarchical Stackelberg Game Model

In this study, a hierarchical Stackelberg game model is established specifically designed for the source-load coordinated optimization problem in a DES. The source side, comprising multiple power plants (leaders), optimizes generation scheduling, while the load side (followers) adjusts energy consumption in response to dynamic carbon emission signals. Unlike traditional Stackelberg models [45], the proposed framework accounts for both economic and environmental objectives, ensuring a balanced trade-off between cost minimization and carbon reduction.

The individual strategy for leader i is signified by x_i, and the composite strategies of all other players, excluding player i, are encapsulated in x_{-i}, and x_{-i} is formally defined as $x_{-i}=\{x_{i'}\mid i'\in U, i'\neq i\}=(x_1,\cdots,x_{i-1},x_{i+1},\cdots,x_N)$. Correspondingly, the strategy for the followers on the load side is characterized by their load response, denoted by $y_i=\{P_t^{\text{lcdr}}\}$.

For the objective functions, the payoff structure φ_i^1 of the source side is detailed in (12). Similarly, the payoff φ_i^2 of the load side is elucidated in (37). The payoff for player i, when employing strategy x_i, is indicated by $\varphi_i(x_i)$, and the collective set of payoffs for all players is given by $\varphi(x)=\{\varphi_i(x_i)\mid i\in U\}$.

Typically, Stackelberg games exhibit inherent power asymmetries, with the leader exerting influence but not fully controlling followers. Each follower independently resolves an optimization problem that considers both the leaders' strategies and those of fellow followers. Consequently, for any given strategy profile $x=(x_1,\cdots,x_N)$, the set of equilibria for the followers is represented by $\mathcal{S}(x_i;x_{-i})=\mathcal{S}(x)$, and y_i is the anticipated strategy profile of all followers from the perspective of leader i [46].

In this Stackelberg game, we assume that an ideal leader would minimize over φ_i^1 while maximizing over φ_i^2. Accordingly, the original objective expressed in (12) can be reformulated for leader i, denoted as $\mathcal{P}_i$:

$$\mathcal{P}_i:\ \min_{x_i,y_i}\varphi_i(x_i,y_i;x_{-i}),\quad \text{s.t.}\ \begin{cases}x_i\in X_i\\ y_i\in\mathcal{S}(x_i;x_{-i})\end{cases} \tag{43}$$

where players independently devise strategies that serve their self-interests, aiming to maximize their respective payoffs. This process continues until a Nash equilibrium is reached, which can be defined as follows.

Definition 1 (Nash equilibrium): A strategy profile $(x^*,y^*)=\{x_i^*,y_i^*\mid i\in U\}$ constitutes a Nash equilibrium when no player can benefit from unilaterally changing their strategy. It is when for every player i, the condition (44) holds true for all x_i, y_i within the strategy set $\mathcal{S}_i$, indicating that there is no incentive for deviation.

$$\varphi_i(x_i^*,y_i^*;x_{-i})\geqslant\varphi_i(x_i,y_i;x_{-i}) \tag{44}$$

2) Quasi-potential Game Algorithm

Prior to identifying a Nash equilibrium in the hierarchical multi-leader multi-follower Stackelberg game we propose, it is essential to verify that the game indeed supports the existence of at least one Nash equilibrium.

Finding a Nash equilibrium can be challenging. Within the realm of non-cooperative games, the QPG is noteworthy, as it guarantees the presence of at least one pure strategy Nash equilibrium [47], characterized by a global quasi-potential function that harmonizes the payoffs for all players. Should a quasi-potential function be established, it would enable the classification of our hierarchical Stackelberg game model as a QPG.

Definition 2 (quasi-potential game): Consider a multi-leader multi-follower game $\mathcal{G}$ in which the objectives of the players are denoted by $\varphi_1,\varphi_2,\cdots,\varphi_N$. $\mathcal{G}$ is a QPG if the following hold:

1) There exists a function $\Phi(\cdot)$ such that for all $i=1,\cdots,N$, $x\in X$ and $x_i\in X_i$, the following equality $\varphi_i(x_i;x_{-i})-\varphi_i(x_i';x_{-i})=\Phi(x_i;x_{-i})-\Phi(x_i';x_{-i})$ holds;

2) For $i=1,\cdots,N$, there exist functions $\phi_1(x),\cdots,\phi_N(x)$ and a function $z(x,y_i)$ such that the objective $\varphi_i(\cdot)$ of each player i is given as $\varphi_i(x_i,y_i;x_{-i})\equiv\phi_i(x)+z(x,y_i)$.

The function Φ serves as the potential function, and the combination $\Phi+z$ is referred to as the quasi-potential function.

Proposition 1*:* The hierarchical Stackelberg game G qualifies as a QPG, with the quasi-potential function being the payoff $\Phi(i)+z$.

Proof: Consider $(x_i, x_i' \in (\varphi_i(x_i)))$ and $x_{-i} \in \varphi_i(x_{-i})$, there is:

$$\Delta\varphi_i = \varphi_i(x_i', x_{-i}) - \varphi_i(x_i, x_{-i}) \tag{45}$$

Similarly, the difference in the potential function can be expressed as:

$$\Delta\Phi = \Phi(x_i', x_{-i}) - \Phi(x_i, x_{-i}) \tag{46}$$

Further expanding this yields:

$$\begin{aligned}\Delta\Phi = \Phi(x_i', x_{-i}) - \Phi(x_i, x_{-i}) = \\ \left[\varphi_i(x_i', x_{-i}) + \sum_{\substack{i' \in U \\ i' \neq i}} \varphi_{i'}(x_{i'})\right] - \\ \left[\varphi_i(x_i, x_{-i}) + \sum_{\substack{i' \in U \\ i' \neq i}} \varphi_{i'}(x_{i'})\right] = \\ \varphi_i(x_i', x_{-i}) - \varphi_i(x_i, x_{-i})\end{aligned} \tag{47}$$

Since $\Delta\varphi_i = \Delta\Phi$ as per condition 1), and the proof for condition 2) follows a similar rationale [48], it proves that the hierarchical Stackelberg game G is a QPG, and $\Phi(i)+z$ serves as a quasi-potential function.

Remark 1: To address the inherent complexity of the multi-leader multi-follower structure, the Stackelberg game is transformed into a QPG, which guarantees the existence of a global equilibrium. The proof (Theorem 3) is constructed by demonstrating that the quasi-potential function $\Phi+z$ satisfies the necessary conditions for convergence in a multi-agent setting. Specifically, in our framework, $\mathcal{G}$ ensures that any unilateral deviation by a single player results in a monotonic change in the potential value, leading to an equilibrium that aligns with optimal energy scheduling strategies. This transformation not only simplifies computation but also provides a theoretically sound method to achieve a stable and efficient solution for the DES.

Theorem 3 (existence of global equilibria of $\mathcal{G}$): Consider $\mathcal{G}$ as a QPG with multi-leaders and multi-followers. Define $\mathcal{U}$ is the set of fixed points (x, y) in the policy space. Assume that $\mathcal{U}$ is a nonempty set and φ_i is a continuous function for each $i \in N$. If there exists a minimizer for $\mathcal{P}$ (for instance, if Φ is a coercive function over $\mathcal{U}$ or if $\mathcal{U}$ is compact), then $\mathcal{G}$ possesses at least one equilibrium.

The existence of a global equilibrium in a Stackelberg game can be proven under certain conditions, which include the continuity [49] and convexity [50] of the objective functions, as well as the non-emptiness [51] of the strategy sets. These conditions are rigorously proven in the cited references, which further establish the existence and consistency of the global equilibrium and a global minimizer. In summary, our proposed hierarchical Stackelberg game G ensures a unique global equilibrium solution and an optimization result.

3) Solution Process

To address carbon reduction challenges in the energy sector, we propose a source-load coordinated optimization framework for DES using a hierarchical Stackelberg game model. In this model, power generation units (leaders) optimize scheduling first, followed by demand-side users (followers) adjusting consumption. To ensure equilibrium and convergence, we transform the multi-leader multi-follower Stackelberg game into a QPG. The optimization follows four iterative steps: 1) source-side economic dispatch; 2) DCEF computation; 3) load-side demand response adjustment; and 4) QPG-based convergence verification. This iterative approach dynamically balances supply and demand, optimizing low-carbon dispatch, maximizing renewable energy utilization, and minimizing system-wide carbon emissions. Algorithm 1 provides a detailed and complete pseudocode and Fig. 5 illustrates the interactive decision-making process within the QPG framework.

Algorithm 1 Source-load Coordination Algorithm Using Quasi-potential Game

Require: Initial strategies $x(0)$, $y(0)$, tolerance ϵ

Ensure: Optimized strategies x^*, y^*

1. Initialize $k=0$, quasi-potential function $\Phi(0)=0$
2. **while** $k<K_{\max}$ **do**
3. Step 1: source optimization (leader's decision)
4. Solve economic dispatch for each unit $i \in X$:
   $x_i(k) = \arg\min_{x_i} \varphi_i^1(x_i, y(k))$
5. Compute updated potential function $\Phi_x(k)$
6. Step 2: compute dynamic carbon emission factor (DCEF)
7. Update system-wide emission factor $F(k)$
8. Step 3: load optimization (follower's decision)
9. Solve demand response for each node $j \in Y$:
   $y_j(k) = \arg\max_{y_j} \varphi_j^2(x(k), y_j)$
10. Compute updated potential function $\Phi_y(k)$
11. Step 4: convergence check
12. **if** $\left|\Phi_x(k) + \Phi_y(k) - \Phi(k-1)\right| < \epsilon$ **then**
13. Store $x^* = x(k)$, $y^* = y(k)$ and break
14. **end if**
15. Update $\Phi(k) = \Phi_x(k) + \Phi_y(k)$, $k \leftarrow k+1$
16. **end while**

Return x^*, y^*

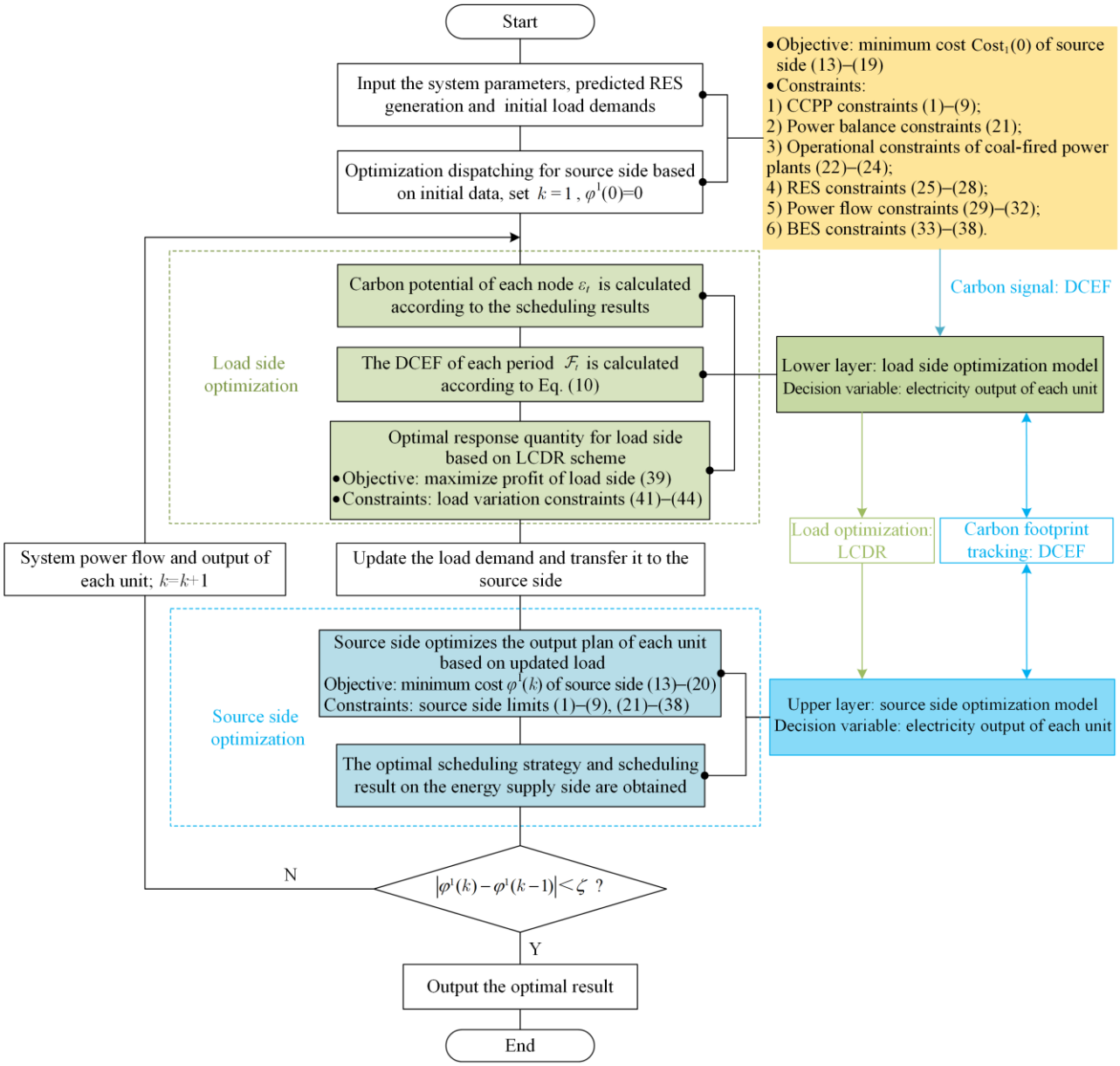

Fig. 5. Flow chart for solving the hierarchical Stackelberg game.

The proposed model involves multiple sources of nonlinearity that require careful treatment to ensure computational tractability. Specifically: 1) Bilinear terms in (14) are linearized using McCormick relaxation; 2) The piecewise function in (18) is reformulated using binary variables; 3) Quadratic generation costs are approximated using piecewise linearization; 4) The bilevel optimization framework is transformed into a QPG to eliminate Stackelberg-level nonlinearity; and 5) The nonlinear constraints in the CCPP model are approximated using first-order Taylor expansion. These transformations ensure that the overall problem can be effectively solved using a combination of MILP and NLP methods [52].

IV. Case Study

In this section, the proposed source-load coordinated scheduling framework is evaluated through case simulations on the modified IEEE39- and IEEE118-node systems. The framework aims to optimize energy distribution and reliability in response to dynamic demand and the integration of RES. the traditional coal-fired power plants, G1 and G2, are transformed into CCPPs within the DES, illustrating this modification in Fig. 6. Furthermore, RES is integrated by introducing six wind farms and three PV installations, with capacities of 200 MW and 150 MW respectively. This integration signifies the framework's adaptability to diverse energy sources, enhancing sustainability. The power forecast

for the electrical load, WT, and PV over a typical day in the DES is illustrated in Fig. 7.

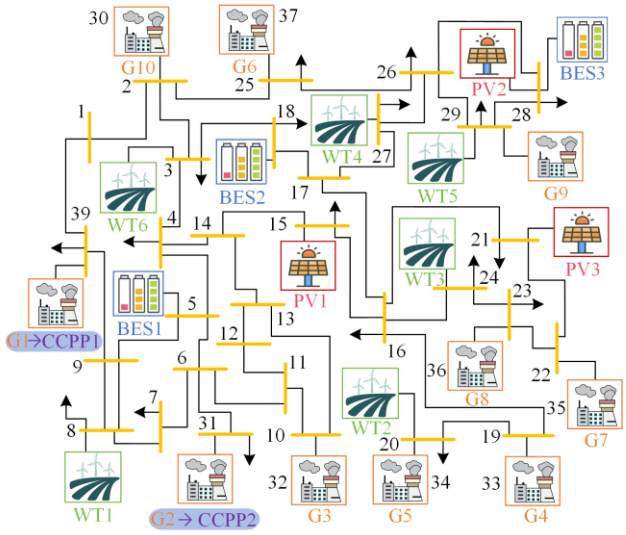

Fig. 6. Modified IEEE39-node system.

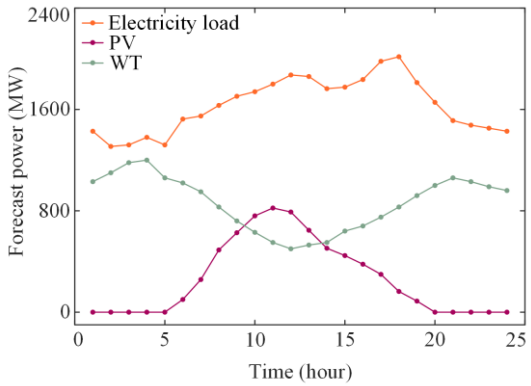

Fig. 7. Forecast power in a typical day.

For simulation purposes, MATLAB (version 2023b) is utilized in conjunction with the YALMIP toolbox and the Gurobi solver (version 10.0.0). With the release of Gurobi 11.0, direct MINLP solving becomes possible [53]. However, to enhance computational efficiency, our hierarchical decomposition approach transforms the MINLP into subproblems that can be solved iteratively. The leader's optimization problem is formulated as an MINLP (solved using Gurobi), while the follower's response, involving nonlinearities from the DCEF calculation, is handled separately using an NLP solver. This structured decomposition ensures computational feasibility while leveraging the latest solver capabilities. To conduct a comparative analysis, six representative cases are selected, as outlined in Table I. In the table, a check mark "√" signifies the inclusion of a specific subsystem, whereas a cross "×" indicates its absence.

TABLE I
SIMULATION CASE

Cases	PDR	LCDR	CCPP (without solution storage)	CCPP (with solution storage)
I	×	×	×	×
II [54]	√	×	×	×
III [55]	×	√	×	×
IV [56]	×	×	√	×
V [6]	×	×	×	√
VI	×	√	×	√

Specifically, the parameters discussed in this study are detailed in Table II. For parameters related to carbon capture, refer to [57]; for renewable energy, see [58]; and for carbon trading, refer to [59]. Data pertaining to each coal-fired power plant (including CCPPs) are presented in Table III.

TABLE II
EXPERIMENTAL PARAMETER SETTING

Parameters	Value	Parameters	Value
ω (MW/t)	0.27	λ ($/t)	14.28
β	0.9	α (%)	20
η (mol/mol)	0.3	ξ (t/MWh)	0.7
φ (kg/t)	1.5	τ_{re} ($/MWh)	20
ρ_{mea} (g/ml)	1.01	τ_{co_2} ($/kg)	1.17
r (%)	8	τ_{so} ($/m^3)	100
τ_{ccs} ($)	2.359 42×10^8	$\mathcal{V}$ (m^3)	60 000×4
Y_1 (a)	15	Y_2 (a)	5

TABLE III
PARAMETERS OF EACH COAL-FIRED UNIT

	P^G_{max} (MW)	P^G_{min} (MW)	τ ($)	a ($/MW^2)/$b$ ($/MW)/$c$ ($)	T_{on}/T_{off} (hour)	R^G_{max} (MW/h)	e^G (t/MW)
G1	455	200	4500	0.000 48/16.2/1000.00	6/6	50	0.9
G2	455	150	5000	0.000 31/17.3/970	5/5	50	0.92
G3	130	30	550	0.002/16.6/700	5/5	25	0.99
G4	130	25	560	0.002 11/16.5/680	5/5	25	0.98
G5	162	45	900	0.003 98/19.7/350	5/5	25	1.02
G6	80	20	170	0.007 12/22.3/370	3/3	18	1.05
G7	85	25	260	0.000 79/27.7/480	3/3	20	1.06
G8	55	10	30	0.004 13/25.9/660	1/1	15	1.12
G9	55	10	30	0.002 22/27.3/665	1/1	15	1.15
G10	55	10	30	0.001 73/27.8/670	1/1	15	1.1

A. Analysis of Scheduling Results

Analysis of Case I reveals that without carbon capture capabilities, DES reaches its peak in both carbon emissions and the RES curtailment rate. This inability to capture CO_2 from power plants prevents the system from earning revenue through the sale of additional carbon allowances, resulting in the highest carbon emission costs.

The introduction of PDR in Case II significantly increases the system's RES output, thereby reducing its carbon emissions. Although this approach compensates for the load during peak periods with additional RES in low periods, the effect of carbon reduction is limited and RES still experiences curtailment. This suggests that the system's low-carbon potential requires further investigation in this case.

In Case III, the load side introduces LCDR, which utilizes DCEF as signals to assist users in modifying their energy consumption behaviors. At first, the effects of LCDR are similar to those of PDR in Case II. However, the advantage of LCDR is that it allows users to directly understand the carbon emissions associated with their electricity use, including those from the supply side. This enables comprehensive tracking of carbon footprints. Figure 8 illustrates the guidance signals of PDR and LCDR, as well as a comparison of their respective load transfer effects. Although the introduction of LCDR alone can shift some of the load, it still faces situations with high carbon emissions. Therefore, it is necessary to consider the combination of LCDR with the deployment of CCPPs.

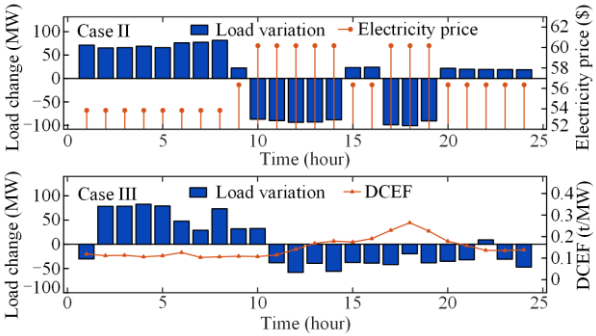

Fig. 8. Compare PDR in Case II with LCDR in Case III.

In Case IV, CCPPs are incorporated on the source side. As illustrated in Fig. 9, the output from CCPPs in Case IV significantly exceeds that of higher carbon-emitting power plants. This leads to the majority of CO_2 emissions within the system being captured and collected by CCS equipment, thus facilitating low-carbon operation of the system. While CCPPs are effective in capturing CO_2 emissions during power generation, they exhibit limited flexibility in adjusting their carbon capture capabilities. They are unable to maximally absorb RES during off-peak periods, indicating that there is still room for optimization.

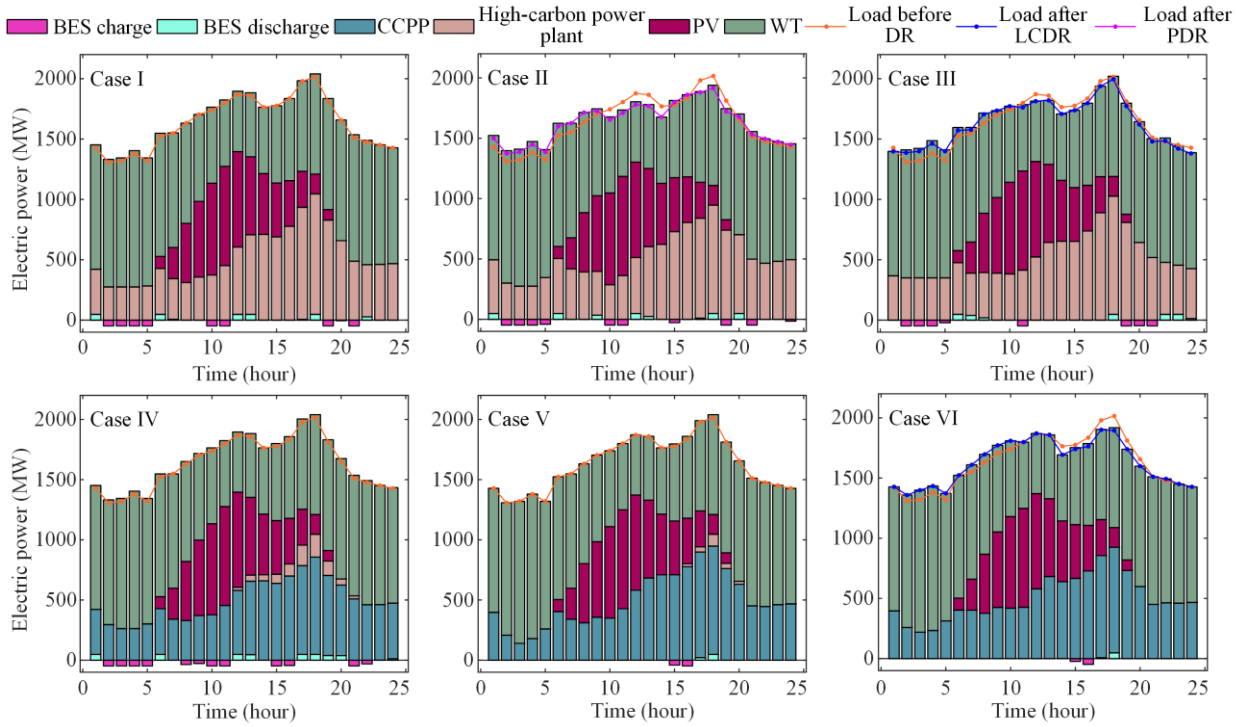

Fig. 9. Total output of electric power in different cases.

In Case V, the CCPPs outfitted with liquid storage tanks can facilitate flexible transfer of carbon capture energy consumption. By storing CO_2 produced during peak periods and capturing it during off-peak periods, this approach offers two primary advantages: first, it can increase the net output of CCPPs during peak periods to

meet load demand; and second, it allows for a reduction in the minimum net output of CCPPs in off-peak periods to absorb more RES power. The scheduling results indicate that this strategy significantly enhances the low-carbon operation of the system. However, some high-carbon power plants still need to operate during peak periods, and the system continues to experience instances of RES curtailment.

The proposed framework in Case VI offers further improvements over the deficiencies identified in the previous cases. By shifting loads from peak to off-peak periods and replacing high-carbon generation during peak times with low-carbon alternatives during off-peak hours, a more substantial reduction in carbon emissions can be achieved. In comparison with Case I, Case III, and Case V, carbon emissions in these cases are reduced by 87.6%, 87.2%, and 16%, respectively. The simulation results demonstrate that the load demand is primarily met by the output from low-carbon units, i.e., CCPPs and RES units.

The optimized scheduling results including the RES curtailment rate θ for various cases are presented in Table IV. Compared to Case I, the RES curtailment rates in Cases II and III, which utilize PDR and LCDR respectively, are reduced by 2.32% and 2.15%, respectively, demonstrating similar impacts on RES consumption. Notably, Case IV, which employs the CCPP diversion mode, exhibits a 2.95% reduction in RES curtailment, 1.19% lower than that of Case I. This decrease is attributed to the operation of low-carbon power plants CCPP1 and CCPP2, which consume electrical energy for CO_2 capture during periods of low demand, thereby reducing the power plant's minimum net output and enhancing RES absorption. Further, Case V incorporates a solution storage to improve carbon capture flexibility, capturing CO_2 during peak periods for use in times of low demand. This strategy effectively lowers the power plant's net output limit, increases RES generation efficiency, and achieves a 4.13% reduction in the RES curtailment rate compared to Case I. Finally, Case VI demonstrates the complete utilization of RES in every period, highlighting the effectiveness of the proposed method in optimizing RES consumption.

TABLE IV
OPTIMIZED SCHEDULING RESULTS IN DIFFERENT CASES

Cases	F_{es} ($)	E_{ac} (t)	θ (%)
I	452 458.41	13 078.64	4.14
II	435 789.82	12 590.43	1.82
III	438 923.11	12 622.04	1.99
IV	438 754.03	3792.82	2.95
V	421 002.55	1924.36	0.03
VI	419 672.27	1616.47	0

To precisely quantify the output of RES across different cases, the RES curtailment rate θ is introduced. The mathematical formulation for this rate is as follows:

$$\theta = \sum_{t=1}^{24} \sum_{i=1}^{N_{res}} \frac{(\hat{P}_{i,t} - P_{i,t}^{res})}{\hat{P}_{i,t}} \tag{48}$$

Figure 10 illustrates the impact of varied cases on RES utilization efficiency, showcasing the differential RES curtailment levels observed from Cases I to Cases VI. Remarkably, Case VI achieves a consistent 100% RES utilization, enabled by the coordinated use of CCPPs and LCDR. LCDR enhances off-peak load absorption of RES, while CCPPs' flexible operation maximizes CO_2 capture during low-demand periods. This coordinated framework effectively reduces the power plant's net output limit and ensures full RES integration by eliminating wastage, illustrating a significant stride towards optimized RES management.

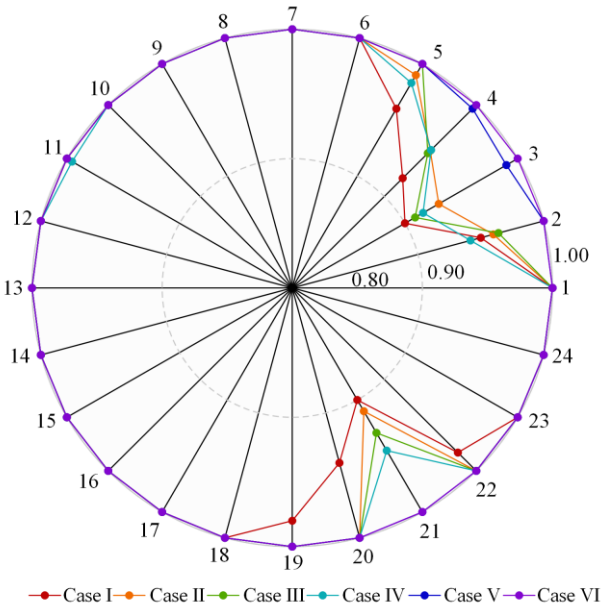

Fig. 10. RES utilization rate in different periods.

To sum up, the proposed method serves as a strategic integration of source-side innovations with LCDR in the load-side to enhance the DES's energy supply efficiency and sustainability. Based on the analysis and scheduling outcomes discussed, it is evident that the proposed source-load coordinated optimization framework demonstrates a comprehensive method to minimizing carbon emissions while ensuring economic viability and maximizing the utilization of RES.

The rate of convergence is further analyzed under the assumption that the utility functions are Lipschitz continuous with a smooth gradient:

$$\|\nabla\varphi_i(x) - \nabla\varphi_i(y)\| \leq L\|x - y\| \tag{49}$$

where L is the Lipschitz constant. Given this smoothness property, it establishes that:

1) If a constant step size η is used, the algorithm exhibits linear convergence.

$$\|x^{(k)} - x^*\| \leq O(1/k) \tag{50}$$

where $x^{(k)}$ denotes the solution at the kth iteration; while x^* represents the global optimal solution; and the notation $O(1/k)$ characterizes the asymptotic upper bound of convergence error, indicating that the error decreases proportionally to $1/k$.

2) If an optimal diminishing step size $\eta_k = \frac{1}{Lk}$ is applied, the algorithm achieves superlinear convergence.

$$\left\|x^{(k)} - x^*\right\| \leqslant O(1/k^2) \tag{51}$$

Figure 11 and Remark 2 are added to explicitly address the convergence rate and future expectations.

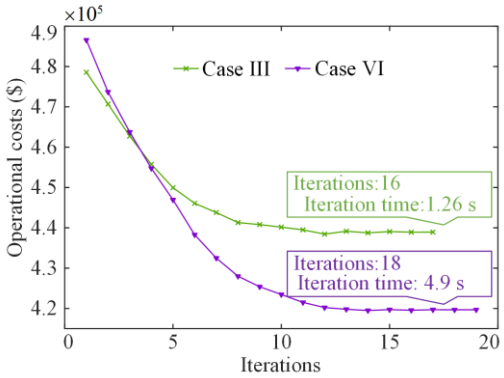

Fig. 11. Convergence of the objective function over iterations.

Remark 2: The proposed QPG method (Case VI) exhibits faster convergence and improved computational efficiency compared to the LCDR method (Case III). Specifically, QPG converges in 18 iterations with an iteration time of 4.9 s, whereas LCDR converges in 16 iterations but with a significantly lower iteration time of 1.26 s. Despite requiring slightly more iterations, the total solving time of QPG remains competitive, benefiting from its structured decomposition. After 30 iterations, the total solution time remains well below that of centralized methods, confirming that the QPG approach efficiently decomposes the high-dimensional MISOCP into tractable subproblems, resulting in improved computational performance. The observed superlinear convergence further highlights the advantage of QPG in complex optimization problems.

To comprehensively evaluate the proposed approach, the proposed QPG algorithm is compared with centralized MISOCP, ADMM [60], and non-cooperative game method, as shown in Table V. The results demonstrate that the proposed QPG algorithm achieves faster convergence (18 iterations vs. 25–30 iterations for other methods), while maintaining high-quality solutions. Compared to the centralized MISOCP algorithm, QPG not only reduces solving time (4.9 s vs. 6.76 s) but also significantly lowers computational complexity, making it more suitable for large-scale systems. Notably, while the number of iterations for QPG is comparable to the centralized method, its computational efficiency is greatly enhanced due to its superlinear convergence property, which enables effective decomposition of the high-dimensional MISOCP problem. QPG outperforms the non-cooperative game method in terms of scalability and overall computational cost, demonstrating its superiority in handling large-scale optimization problems. These findings confirm the cost-effectiveness and efficiency of the proposed QPG framework in addressing complex energy scheduling challenges.

TABLE V
COMPARATIVE RESULTS

Case	Iterations	Solution time (s)	Results ($)
Centralized algorithm		6.76	431 897.51
ADMM	30	7.48	423 285.59
Non-cooperative game	25	6.3	427 035.83
QPG	18	4.9	419 672.27

B. Analysis of Robustness

Considering the fact that renewable energy output and load demand are random, this paper quantitatively analyzes the influence of renewable energy output fluctuation, intermittence and load demand fluctuation on the optimization results by using random scene analysis method [61].

According to the current research [62] conclusions on renewable energy output and load forecasting, it can be set that the output and load forecasting of renewable energy should meet the following models:

$$P_n^t = \bar{P}_n^t (1 + e_n^{\max} \times R_n\{-1,1\}) \tag{52}$$

where n=1, 2, 3, represent WT, PV and load demand (LD), respectively; P_n^t is the forecast data of the time t period; and $\bar{P}_n^t$ is the historical data of the time t period; $R_n\{-1,1\}$ is a random number with a value from 1 to –1; while $e_n^{\max}$ is the maximum uncertainty percentage, which can be expressed as:

$$e_n^{\max} = K \times e_n^{\text{basic}} \tag{53}$$

where K is uncertainty grade, and is set as 1, 3, 5, 7, 9; e_n^{basic} means basic uncertainty, while WT is set as 3%, PV as 2% and LD as 1%.

The above uncertainties are added to the predicted initial values of WT, PV and LD, and 60 random scenarios are set up. In addition, the concept of load volatility is introduced as:

$$V(t) = \frac{\sigma(\Delta N(t))}{\mu(N(t))} \tag{54}$$

where $N(t)$ represents net load, which is obtained by subtracting the renewable energy generation from the total power demand at time t; $\Delta N(t)$ means the variation of net load; while the net load volatility $V(t)$ can be obtained by calculating the standard deviation of the

net load variation $\sigma(\Delta N(t))$ and the average value of the net load $\mu(N(t))$.

Additional simulations are conducted under different levels of renewable energy intermittency and demand variations. Figures 12 and 13 show that the proposed QPG maintains stable convergence and solution quality, demonstrating its resilience against uncertainties. In addition, the proposed method further benchmarked against traditional deterministic optimization and adaptive strategies, confirming that the proposed approach provides a more balanced trade-off between computational efficiency and robustness in uncertain environments. The specific analysis is as follows.

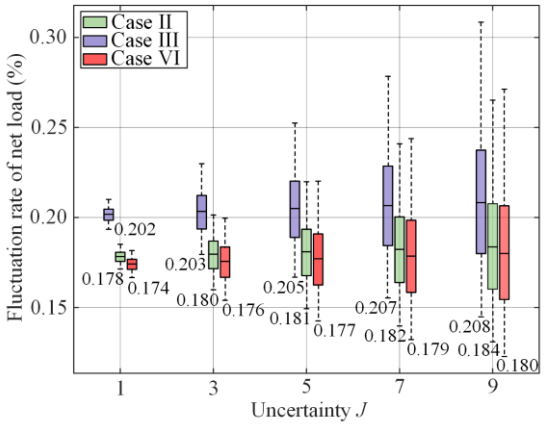

Fig. 12. Comparison of net load fluctuation rate in different cases after rolling optimization under various uncertainties.

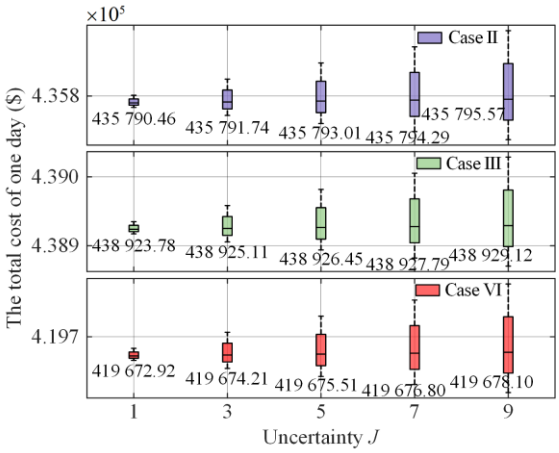

Fig. 13. Comparison of total cost of each case after rolling optimization under various uncertainties.

In the six typical cases, the focus is on comparing Case II, Case III, and Case VI to provide a more intuitive reflection of the optimization results. As shown in Figs. 12 and 13, under various uncertainties, Case VI, after rolling optimization, demonstrates significant improvements in net load volatility and economic efficiency compared to Case II and Case III. As uncertainty increases, net load volatility rises while economic efficiency declines. However, Case VI exhibits greater resilience to uncertainty, with a slower increase in net load volatility and a more gradual decline in economic performance. This confirms the effectiveness of our day-ahead optimization algorithm in mitigating uncertainty impacts. For instance, at an uncertainty level of 5, the net load volatility of Case VI is reduced by approximately 0.028% and 0.004% compared to Case II and Case III, respectively, while the total cost is reduced by approximately $ 16 117.52 and $ 19 250.94. Additionally, for every two-level increase in uncertainty, the net load volatility increases by approximately 0.0016% in Case II, 0.0013% in Case III, and 0.0014% in Case VI, while the total cost increases by about $ 1.28, $ 1.33, and $ 1.28, respectively. These findings further validate the effectiveness and robustness of the proposed QPG optimization algorithm (Case VI) in improving system stability and economic efficiency under uncertainty.

C. Analysis of Low-carbon Optimization Results

The variations in the DCEF and optimized carbon emissions across different cases are depicted in Fig. 14. This illustration demonstrates that the application of demand response (DR) strategies on the load side, particularly in Cases II and III, effectively mitigates peak-period carbon emissions. Nevertheless, these cases demonstrate a continued dependence on high-carbon power units, resulting in increased CO_2 emissions during low-demand periods despite the implementation of DR strategies.

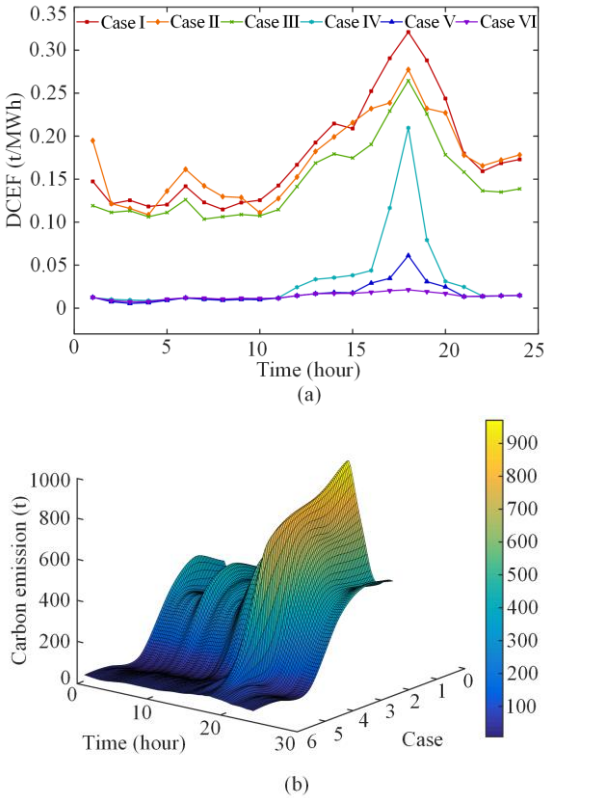

Fig. 14. Comparison of optimized carbon emissions results. (a) Carbon emissions factor in each case. (b) Carbon emissions in each case.

Despite the significant reduction in system CO_2 emissions achievable with a shared-mode carbon capture device, its limited capture capacity prevents it from fully meeting the low-carbon requirements of the DES. In contrast, Case V, which builds upon Case IV with the addition of solution storage, enhances the flexibility of carbon capture. This allows for CO_2 capture at any time, thereby further reducing system carbon emissions.

Case VI, which augments Case V with LCDR, stands out by transferring peak-period loads to reduce high-carbon power plant outputs. These are replaced by lower carbon outputs from CCPP1 and CCPP2 during off-peak periods. As a result, Case VI exhibits the lowest carbon emissions. This analysis validates the effectiveness of the proposed source-load coordinated low-carbon scheduling framework (Case VI) in achieving substantial reductions in carbon emissions.

To further investigate the influence of carbon trading prices on the DES, we analyze variations in total carbon emissions and associated costs under diverse scenarios at different levels of carbon trading price.

The relationship between carbon emissions and carbon base prices under each scenario is depicted in Fig. 15. The data reveal that the trends in carbon emissions for Cases I–III remain relatively stable. This stability suggests that when carbon revenue falls below the cost of carbon capture, CCPPs choose to release the CO_2 into the atmosphere rather than to capture it. When the carbon price is below $ 9, the emissions in Case VI exceed those in Case V. This outcome can be attributed to CCPP1 and CCPP2 operating at their minimum output limits, a decision driven by low carbon revenue and the significant costs associated with starting up and shutting down these plants during periods of low demand. In Case V, despite these constraints, CCPP1 and CCPP2 are still able to capture CO_2 subsequent to fulfilling the system's load demands and addressing the curtailment of RES. In Case VI, the deployment of LCDR increases the off-peak load to a level where the output of CCPP1 and CCPP2 merely satisfies the load demand, rendering it insufficient for carbon capture.

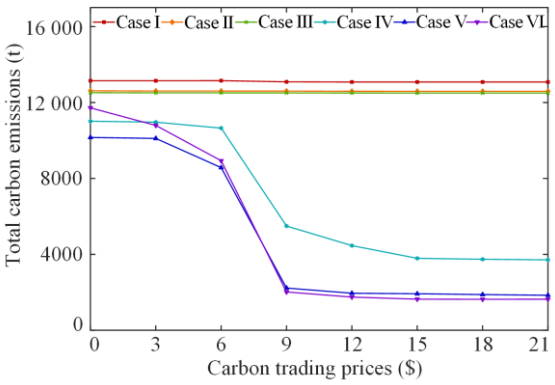

Fig. 15. The carbon emissions at different carbon prices.

Figure 16 illustrates how the total cost of the system in case VI varies with the base carbon price. This case exhibits an initial increase and subsequent decrease in total cost as the carbon price changes. When the carbon price is below $ 9, the rate at which carbon emissions decrease is slower than the rate at which the carbon price increases. As a result, the carbon emission cost in Case VI trends upward under this threshold.

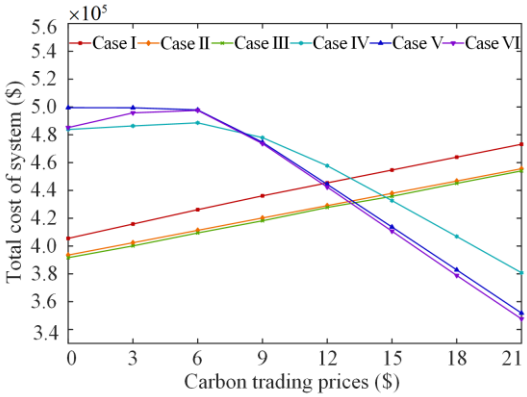

Fig. 16. The total cost at different carbon prices.

Furthermore, Case VI consistently maintains a lower total cost compared to Case V across various carbon prices. This is primarily due to the implementation of LCDR in Case VI, which reduces the reliance on higher-cost, high-carbon power plants. As indicated in Table IV, the operational costs of these high-carbon power plants are considerably higher than those of CCPP. Therefore, despite having higher carbon emissions than Case V, Case VI still achieves a lower overall cost due to reduced expenses associated with high-carbon power plant outputs.

D. Scalability Verification for Large-scale Bus Systems

To confirm the practical feasibility of our proposed framework and algorithm in real-world power systems and other complex large-scale environments, we employ the IEEE118-node power system as a case study for performance evaluation. The bus model, conforming to the rigorous IEEE118-node specifications, enables a detailed examination of our source-load coordinated low-carbon economic scheduling framework, which integrates the LCDR method. For a comprehensive evaluation, we compare the performance outcomes of our framework using the IEEE39-node model as a benchmark. The comparative analysis, focusing on the performance of Cases III and VI across the IEEE39- and IEEE118-nodes, is detailed in Table VI.

TABLE VI
SOLUTION TIME

Benchmark	Cases	Iterations	Solution time (s)
IEEE39	III	16	1.26
	VI	18	4.9
IEEE118	III	18	6.12
	VI	21	11.59

The data presented in the table indicate that the solution time for our proposed framework exhibits a linear increase as the system scale expands, demonstrating commendable scalability in large-scale power systems. Compared to Case III, our framework necessitates additional iterations and longer solution times. This increase can be attributed to the integration of CCPPs on the load side for carbon capture, which, despite adding complexity, yields significant improvements in carbon capture efficiency and economic scheduling outcomes.

The carbon capture efficiency within the IEEE118-node system for Case IV, Case V, and Case VI is depicted in Fig. 17. During peak load periods in the daytime, the DES in Case IV struggles to manage the abrupt increase in load demand without the supportive capacity of a solution storage tank. In contrast, Case VI, which incorporates the LCDR, achieves superior carbon capture efficiency, outperforming Case V by 4.6%.

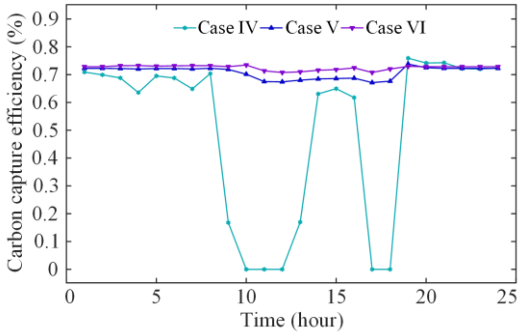

Fig. 17. Carbon capture efficiency in IEEE118-node system.

In conclusion, the introduced source-load coordinated low-carbon system demonstrates notable carbon capture efficiency within the IEEE118-node system. Furthermore, our proposed framework exhibits adequate scalability and applicability for large-scale complex systems, underscoring its potential as a robust solution for enhancing low-carbon initiatives in DES.

V. Conclusion

In this paper, a source-load coordinated optimization framework for DES is proposed, integrating CCPPs on the source side and the LCDR method on the load side. The original hierarchical multi-leader multi-follower Stackelberg game problem is transformed into a QPG model, and the existence and consistency of the Nash equilibrium are proved. The proposed algorithm achieves good convergence and scalability.

Simulation results on IEEE39- and IEEE118-node systems show that, compared to the benchmark Case I, the proposed Case VI reduces carbon emissions by 87.6%, eliminates RES curtailment, and achieves the lowest system cost. Moreover, the QPG algorithm converges in 18 iterations with a solution time of 4.9 s, outperforming traditional methods. These results validate the effectiveness and robustness of the proposed framework in realizing low-carbon, efficient, and scalable scheduling for DES.

Acknowledgment

Not applicable.

Authors' Contributions

Guofeng Wang: full-text writing and the construction of the paper framework. Bei Jiang and Yuchen Liu: software and simulations. Licheng Wang: conceptualization, methodology, and data curation. Youbing Zhang: conceptualization and methodology. Jun Yan: reviewing and editing. Kai Wang: reviewing, editing, and supervising. All authors read and approved the final manuscript.

Funding

This work is supported by the National Natural Science Foundation of China (No. U22B20116); Young Elite Scientist Sponsorship Program of Zhejiang Association for Science and Technology; and China Scholarship Council.

Availability of Data and Materials

Not applicable.

Declarations

Competing interests: The authors declare that they have no known competing financial interests or personal relationships that could have appeared to influence the work reported in this article.

Authors' Information

Guofeng Wang was born in Zhejiang, China, in 1993. He received his B.S. degree from Kunming University of Science and Technology in 2015, and his Ph.D. degree in Control Science and Engineering from Zhejiang University of Technology in 2021. From 2021 to 2024, he worked as an assistant researcher at Zhejiang University of Technology. From 2023 to 2024, he also conducted postdoctoral research at Concordia University, Canada. He is currently a lecturer (assistant professor) at Zhejiang University of Technology. His research interests include integrated energy systems, low-carbon power systems, and AI-based scheduling and optimization.

Bei Jiang received the B.Eng. degree in automation from the Nanjing University of Science and Technology ZiJin College, in 2023. She is currently pursuing the M.S. degree in control science and engineering with the Zhejiang University of Technology. Her research interests include power system optimization and operation.

Yuchen Liu received M.S. degree in control science and engineering from Zhejiang University of Technology in 2024. His research focuses on low-carbon optimization of power systems and low-carbon operation scheduling of integrated energy systems.

Licheng Wang works at the College of Information Engineering, Zhejiang University of Technology, Hangzhou, China. His research interests include power system operation and control, renewable energy integration into distribution systems, distributed algorithms, deep reinforcement learning and its application in networked systems.

Youbing Zhang received the B.S. and M.S. degrees in electrical engineering from Hunan University, Changsha, China, in 1993 and 1996, respectively, and the Ph.D. degree in electrical engineering from Huazhong University of Science and Technology, Wuhan, China, in 2003. From 1996 to 1997, he was a research assistant both at Tsinghua University, Beijing, China, and China Electric Power Research Institute, Beijing, China. From 1997 to 1999, he was a lecturer at the Department of Electrical Engineering in Hunan University. From 2003 to 2005, he was a postdoctoral research fellow at the Zhejiang University, Hangzhou, China. He is currently a professor with the College of Information Engineering, Zhejiang University of Technology, Hangzhou, China. His research interests include demand-side management, vehicle-to-grid technology, power quality monitoring and control, smart energy, and big data applications.

Jun Yan received the Ph.D. degree (with excellence in doctoral research) in electrical engineering from the University of Rhode Island, Kingston, RI, USA, in 2017. He is currently an associate professor and the University Research Chair (Tier 2) on Artificial Intelligence in Cyber Security and Resilience with the Concordia Institute for Information Systems Engineering, Concordia University, Montréal, QC, Canada. He co-directs the Concordia Digital Twins Hub and the NSF EuReCa Center on Equitable, Resilient, and Clean Energy for Grid Interactive Communities. His current research interests include computational intelligence, security, and resilience for cyber-physical systems in smart grids, smart cities, and other smart critical infrastructures. Dr. Yan was the recipient of the Best Paper Award of IEEE ICC, the Best Student Paper Award of IEEE WCCI, the Best Readings of IEEE ComSoc, and several other awards.

Kai Wang works at the School of Electrical Engineering, Qingdao University, Shandong province, China. His research interests include state assessment and life prediction of new energy storage devices, energy storage element, storage and conversion of new energy.

REFERENCES

[1] J. Han, W. Wang, and C. Yang *et al*., "FRMNet: a feasibility restoration mapping deep neural network for AC optimal power flow," *IEEE Transactions on Power Systems*, vol. 39, no. 5, pp. 6566-6577, Sept. 2024.

[2] D. I. A. McKay, A. Staal, and J. F. Abrams *et al*., (2022, Sept.), "Exceeding 1.5°C global warming could trigger multiple climate tipping points," *Science*, [Online], 377 (6611). Available: https://www.science.org/doi/abs/10.1126/science.abn7950

[3] D. Shu, S. Deutz, and B. A. Winter *et al*., "The role of carbon capture and storage to achieve net-zero energy systems: trade-offs between economics and the environment," *Renewable and Sustainable Energy Reviews*, vol. 178, May 2023.

[4] T. Wilberforce, A. Olabi, and E. T. Sayed *et al*., "Progress in carbon capture technologies," *Science of the Total Environment*, vol. 761, Mar. 2021.

[5] G. Wang, B. Jiang, and S. Dong *et al*., "A market-oriented trading method for integrated community energy system based on hierarchical Stackelberg game method," *International Transactions on Electrical Energy Systems*, vol. 2024, pp.1-17, Nov. 2024.

[6] A. Akbari-Dibavar, B. Mohammadi-Ivatloo, and K. Zare *et al*., "Economic-emission dispatch problem in power systems with carbon capture power plants," *IEEE Transactions on Industry Applications*, vol. 57, no. 4, pp. 3341-3351, May 2021.

[7] L. Wang, T. Wang, and G. Huang *et al*., "Softly collaborated voltage control in PV rich distribution systems with heterogeneous devices," *IEEE Transactions on Power Systems*, vol. 39, no. 4, pp. 5991-6003, Jul. 2023.

[8] G. Qi, N. Ma, and K. Wang, "Predicting the remaining useful life of supercapacitors under different operating conditions," *Energies*, vol. 17, no. 11, May 2024.

[9] G. Zhang, W. Wang, and Z. Chen *et al*., "Modeling and optimal dispatch of a carbon-cycle integrated energy system for low-carbon and economic operation," *Energy*, vol. 240, Feb. 2022.

[10] A. Xuan, X. Shen, and Q. Guo *et al*., "Two-stage planning for electricity-gas coupled integrated energy system with carbon capture, utilization, and storage considering carbon tax and price uncertainties," *IEEE Transactions on Power Systems*, vol. 38, no. 3, pp. 2553-2565, May 2023.

[11] Y. Jiang, Z. Ren, and W. Li, "Committed carbon emission operation region for integrated energy systems: Concepts and analyses," *IEEE Transactions on Sustainable Energy*, vol. 15, no. 2, pp. 1194-1209, Apr. 2024.

[12] L. Ju, Z. Yin, and X. Lu *et al*., "A tri-dimensional equilibrium-based stochastic optimal dispatching model for a novel virtual power plant incorporating carbon capture, power-to-gas and electric vehicle aggregator," *Applied Energy*, vol. 324, Oct. 2022.

[13] Council of the State Council of China. (2021, Oct. 27). *Action Plan for Carbon Dioxide Peaking Before 2030*. [Online]. Available: http://www.xinhuanet.com/english/download/2021-10-27/FullTextActionPlanforCarbonDioxidePeakingBefore2030.doc

[14] Environment and Climate Change Canada. (2022, Mar. 29). *2030 Emissions Reduction Plan-Canada's next Steps for Clean Air and a Strong Economy*. [Online]. Available: https://www.canada.ca/en/environment-climate-change/news/2022/03/2030-emissions-reduction-plan--canadas-next-steps-for-clean-air-and-a-strong-economy.html

[15] S. Zheng, Y. Sun, and B. Qi *et al*., "Incentive-based integrated demand response considering s&c effect in demand side with incomplete information," *IEEE Transactions on Smart Grid*, vol. 13, no. 6, pp. 4465-4482, Nov. 2022.

[16] B. Yu, F. Sun, and C. Chen *et al*., "Power demand response in the context of smart home application," *Energy*, vol. 240, Feb. 2022.

[17] C. Li, Z. Yan, and Y. Yao *et al*., "Coordinated low-carbon dispatching on source-demand side for integrated electricity-gas system based on integrated demand response exchange," *IEEE Transactions on Power Systems*, vol. 39, no. 1, pp. 1287-1303, Jan. 2024.

[18] D. Yang, Y. Xu, and X. Liu *et al*., "Economic-emission dispatch problem in integrated electricity and heat system considering multi-energy demand response and carbon capture technologies," *Energy*, vol. 253, no. 1, Feb. 2022.

[19] T. Niu, H. Li, and G. Chen *et al*., "Pricing and distributed scheduling framework of multi-microgrid system based on coupled electricity-carbon market," *Journal of Modern Power Systems and Clean Energy*, vol. 13, no. 3, pp. 1-13, Oct. 2024.

[20] Y. Zou, Y. Xu, and C. Zhang, "A risk-averse adaptive stochastic optimization method for transactive energy management of a multi-energy microgrid," *IEEE Transactions on Sustainable Energy*, vol. 14, no. 3, pp. 1599-1611, Jul. 2023.

[21] Z. Wang, H. Hou, and B. Zhao, *et al*. "Risk-averse stochastic capacity planning and p2p trading collaborative optimization for multi-energy microgrids considering carbon emission limitations: an asymmetric nash bargaining approach," *Applied Energy*, vol. 357, Mar. 2024.

[22] J. Lin, C. Gao, and J. Zeng *et al*., "Stackelberg-nash asymmetric bargaining-based scheduling optimization and revenue-allocation for multi-operator regional integrated energy system considering competition-cooperation relationship and source-load uncertainties," *Energy*, vol. 291, Mar. 2024.

[23] J. Nie, B. Jiang, and Z. Lan *et al*., "Low-carbon economic dispatch for distributed energy system using quasi-potential game," in *2024 IEEE 8th Conference on Energy Internet and Energy System Integration (EI2)*, Shenyang, China, Nov. 2024, pp. 448-453.

[24] K. Zhang, H. C. Lau, and H. K. Bokka *et al*., "Decarbonizing the power and industry sectors in india by carbon capture and storage," *Energy*, vol. 249, Jun. 2022.

[25] L. Yin and M. Tao, "Balanced broad learning prediction model for carbon emissions of integrated energy systems considering distributed ground source heat pump heat storage systems and carbon capture storage," *Applied Energy*, vol. 329, Jan. 2023.

[26] C. K. Chyong, D. M. Reiner, and R. Ly *et al*., "Economic modelling of flexible carbon capture and storage in a decarbonised electricity system," *Renewable and Sustainable Energy Reviews*, vol. 188, Dec. 2023.

[27] M. Wu, J. Xu, and Z. Shi, "Low carbon economic dispatch of integrated energy system considering extended electric heating demand response," *Energy*, vol. 278, Sep. 2023.

[28] C. Duan, G. Bharati, and P. Chakraborty, *et al*. "Practical challenges in real-time demand response," *IEEE Transactions on Smart Grid*, vol. 12, no. 5, pp. 4573-4576, Sep. 2021.

[29] J. Ruan, G. Liang, and J. Zhao *et al*., "Graph deep-learning-based retail dynamic pricing for demand response," *IEEE Transactions on Smart Grid*, vol. 14, no. 6, pp. 4385-4397, Nov. 2023.

[30] X. Zhang, Z. Guo, and F. Pan *et al*., "Dynamic carbon emission factor based interactive control of distribution network by a generalized regression neural network assisted optimization," *Energy*, vol. 283, Nov. 2023.

[31] J. Li, G. Wang, and X. Wang *et al*., "Smart charging strategy for electric vehicles based on marginal carbon emission factors and time-of-use price," *Sustainable Cities and Society*, vol. 96, Sep. 2023.

[32] N. Yan, G. Ma, and X. Li *et al*., "Low-carbon economic dispatch method for integrated energy system considering seasonal carbon flow dynamic balance," *IEEE Transactions on Sustainable Energy*, vol. 14, no. 1, pp. 576-586, Jan. 2023.

[33] Z. Lü, H. Du, and S. Xu *et al*., "Techno-economic analysis on CO_2 mitigation by integrated carbon capture and methanation," *Applied Energy*, vol. 355, Feb. 2024.

[34] J. Asadi and P. Kazempoor, "Advancing power plant decarbonization with a flexible hybrid carbon capture system," *Energy Conversion and Management*, vol. 299, Jan. 2024.

[35] P. Jiao, X. Cai, and L. Wang *et al*., "Flexibility operation for integrated energy system considering hydrogen energy under inertia characteristics and stepped carbon trading mechanism," *Sustainable Cities and Society*, vol. 98, Nov. 2023.

[36] J. Gao, D. Yang, and S. Wang *et al*., "State of health estimation of lithium-ion batteries based on mixers-bidirectional temporal convolutional neural network," *Journal of Energy Storage*, vol. 73, Dec. 2023.

[37] N. Cao, H. Du, and J. Lu *et al*., "Designing ionic liquid electrolytes for a rigid and Li^+-conductive solid electrolyte interface in high performance lithium metal batteries," *Chemical Physics Letters*, vol. 866, May 2025.

[38] Y. Pan, K. Xu, and R. Wang *et al*., "Lithium-ion battery condition monitoring: A frontier in acoustic sensing technology," *Energies*, vol. 18, no. 5, Dec. 2025.

[39] Y. Xiang, Y. Guo, and G. Wu *et al*., "Low-carbon economic planning of integrated electricity-gas energy systems," *Energy*, vol. 249, Jun. 2022.

[40] X. Zhong, W. Zhong, and Y. Liu *et al*., "Optimal energy management for multi-energy multi-microgrid networks considering carbon emission limitations," *Energy*, vol. 246, May 2022.

[41] Y. Liu, Q. Li, and K. Wang, "Revealing the degradation patterns of lithium-ion batteries from impedance spec-

troscopy using variational auto-encoders," *Energy Storage Materials*, vol. 69, May 2024.

[42] Y. Zhu, S. Zhang, and Q. Xu *et al*., "Source load bilateral cooperative game scheduling considering LCA carbon emissions," *Power System Protection and Control*, vol. 52, no. 2, pp. 48-58, Jan. 2024. (in Chinese)

[43] A. Agarwal, A. Pandey, and L. Pileggi, "Continuous switch model and heuristics for mixed-integer nonlinear problems in power systems," *IEEE Transactions on Power Systems*, vol. 39, pp. 5780-5791, Jul. 2023.

[44] J. Wang, X. Dai, and D. Cheng, "Quasi-potential game," *IEEE Transactions on Circuits and Systems II: Express Briefs*, vol. 69, no. 11, pp. 4419-4422, Nov. 2022.

[45] Y. Zang, S. Xia, and J. Li *et al*., "A robust game optimization scheduling method for shared energy storage micro electric network group distribution," *Power System Protection and Control*, vol. 51, no. 24, pp. 90-101, Dec. 2023. (in Chinese)

[46] A. A. Kulkarni and U. V. Shanbhag, "An existence result for hierarchical stackelberg v/s stackelberg games," *IEEE Transactions on Automatic Control*, vol. 60, no. 12, pp. 3379-3384, Dec. 2015.

[47] D. Monderer and L. S. Shapley, "Potential games," *Games and Economic Behavior*, vol. 14, no. 1, pp. 124-143, May 1996.

[48] X. Gao, R. Liu, and A. Kaushik, "Virtual network function placement in satellite edge computing with a potential game approach," *IEEE Transactions on Network and Service Management*, vol. 19, no. 2, pp. 1243-1259, Jun. 2022.

[49] S. Maharjan, Q. Zhu, and Y. Zhang *et al*., "Dependable demand response management in the smart grid: a Stackelberg game approach," *IEEE Transactions on Smart Grid*, vol. 4, no. 1, pp. 120-132, Mar. 2013.

[50] T. Jiang, C. Y. Chung, and P. Ju *et al*., "A multi-timescale allocation algorithm of energy and power for demand response in smart grids: a Stackelberg game approach," *IEEE Transactions on Sustainable Energy*, vol. 13, no. 3, pp. 1580-1593, Jul. 2022.

[51] K. Anoh, S. Maharjan, and A. Ikpehai *et al*., "Energy peer-to-peer trading in virtual microgrids in smart grids: a game-theoretic approach," *IEEE Transactions on Smart Grid*, vol. 11, no. 2, pp. 1264-1275, Mar. 2020.

[52] H. Li, Z. Ren, and A. Trivedi *et al*., "Optimal planning of dual-zero microgrid on an island toward net-zero carbon emission," *IEEE Transactions on Smart Grid*, vol. 15, no. 2, pp. 1243-1257, Mar. 2024.

[53] Gurobi Optimization. [Online]. Available: http://www.gurobi.com/whats-new-gurobi-11-0/

[54] M. Miri and M. McPherson, "Demand response programs: Comparing price signals and direct load control," *Energy*, vol. 288, Feb. 2024.

[55] T. Wan, Y. Tao, and J. Qiu *et al*., "Internet data centers participating in electricity network transition considering carbon-oriented demand response," *Applied Energy*, vol. 329, Jan. 2023.

[56] L. Zhang, K. Ye, and Y. Z. Wang *et al*., "Performance analysis of a hybrid system combining cryogenic separation carbon capture and liquid air energy storage (CS-LAES)," *Energy*, Mar. 2023.

[57] J. Liu, H. Chen, and S. Zhao *et al*., "Evaluation and improvements on the flexibility and economic performance of a thermal power plant while applying carbon capture, utilization & storage," *Energy Conversion and Management*, vol. 290, Aug. 2023.

[58] C. Chen, Y. Li, and W. Qiu *et al*., "Cooperative-game-based day-ahead scheduling of local integrated energy systems with shared energy storage," *IEEE Transactions on Sustainable Energy*, vol. 13, no. 4, pp. 1994-2011, Oct. 2022.

[59] Y. Wang, J. Hu, and N. Liu, "Energy management in integrated energy system using energy-carbon integrated pricing method," *IEEE Transactions on Sustainable Energy*, vol. 14, no. 4, pp. 1992-2005, Oct. 2023.

[60] G. Wang, Y. Liu, and Y. Zhang *et al*., "Distributed online optimization for integrated energy systems: a multi-agent system consensus approach," *International Journal of Adaptive Control and Signal Processing*, vol. 38, no. 10, pp. 3401-3421, Jun. 2024.

[61] A. Saxena and R. Shankar, "An interactive operating demand response approach for hybrid power systems integrating renewable energy sources," *Protection and Control of Modern Power Systems*, vol. 9, no. 3, pp. 174-194, May 2024.

[62] H. Han, Y. Xu, and C. Wu *et al*., "Nash equilibrium-based two-stage cooperative operation strategy for multi-microgrids considering uncertainty," *Protection and Control of Modern Power Systems*, vol. 9, no. 6, pp. 42-57, Nov. 2024.